Jupiter's auroral-related stratospheric heating and chemistry III: abundances of C_2H_4, CH_3C_2H, C_4H_2 and C_6H_6 from Voyager-IRIS and Cassini-CIRS

J. A. Sinclair[a,*], J. I. Moses[b], V. Hue[c], T. K. Greathouse[c], G. S. Orton[a], L. N. Fletcher[d], P. G. J. Irwin[e]

[a] *Jet Propulsion Laboratory/California Institute of Technology, 4800 Oak Grove Dr, Pasadena, CA 91109, United States*
[b] *Space Science Institute, 4750 Walnut St, Suite 205, Boulder, CO 80301, United States*
[c] *Southwest Research Institute, 6220 Culebra Rd., San Antonio, TX 78236, United States*
[d] *Department of Physics & Astronomy, University of Leicester, University Road, Leicester, LE1 7RH, United Kingdom*
[e] *Atmospheric, Oceanic & Planetary Physics, University of Oxford, Parks Road, Oxford, OX1 3PU, United Kingdom*

Abstract

We present an analysis of Voyager-1-IRIS and Cassini-CIRS spectra of Jupiter's high latitudes acquired during the spacecrafts' respective flybys in November 1979 and January 2001. We performed a forward-model analysis in order to derive the abundances of ethylene (C_2H_4), methylacetylene (CH_3C_2H), diacetylene (C_4H_2) and benzene (C_6H_6) in Jupiter's northern and southern auroral regions. We also compared these abundances to: 1) lower-latitude abundances predicted by the (Moses et al., 2005) 'Model A' photochemical model, henceforth 'Moses 2005A', and 2) abundances derived at non-auroral longitudes in the same latitude band. This paper serves as an extension of Sinclair et al. (2017a), where we retrieved the vertical profiles of temperature, C_2H_2 and C_2H_6 from similar datasets. We find that an enrichment of C_2H_4, CH_3C_2H and C_6H_6 with respect to lower-latitude abundances is required to fit the spectra of Jupiter's northern and southern auroral regions. For example, for CIRS 0.5 cm^{-1} spectra of Jupiter's southern auroral region, scale factor enrichments of $6.40^{+1.30}_{-1.15}$ and $9.60^{+3.98}_{-3.67}$ are required with respect to the Moses 2005A vertical profiles of C_2H_4 and C_6H_6, respectively, in order to fit the spectral emission features of these species at ~950 and ~674 cm^{-1}. Similarly, in order to fit the CIRS 2.5 cm^{-1} spectra of Jupiter's northern auroral region, scale factor enrichments of $1.60^{+0.37}_{-0.21}$, $3.40^{+1.89}_{-1.69}$ and $15.00^{+4.01}_{-4.02}$ with respect to the Moses 2005A vertical profiles of C_2H_4, CH_3C_2H and C_6H_6 were required, respectively.. Outside of Jupiter's auroral region in the same latitude bands, only upper-limit abundances of C_2H_4, CH_3C_2H and C_6H_6 could be determined due to the limited sensitivity of the measurements, the weaker emission features combined with cooler stratospheric temperatures (and therefore decreased thermal emission) of these regions. Nevertheless, for a subset of the observations, derived abundances of C_2H_4 and C_6H_6 in Jupiter's auroral regions were higher (by greater than 1-σ) with respect to upper-limit abundances derived outside the auroral region in the same latitude band. This is suggestive that the influx of energetic ions and electrons from the jovian magnetosphere and external solar-wind environment into the neutral atmosphere in Jupiter's auroral regions drives enhanced ion-related chemistry, as has also been inferred from Cassini observations of Saturn's high latitudes (Guerlet et al., 2015; Koskinen et al., 2016; Fletcher et al., 2018). We were not able to constrain the abundance of C_4H_2 in either Jupiter's auroral regions or non-auroral regions due to its lower (predicted) abundance and weaker emission feature. Thus, only upper-limit abundances were derived in both locations. From CIRS 2.5 cm^{-1} spectra, the upper limit abundance of C_4H_2 corresponds to a scale factor enhancement of 45.6 and 23.8 with respect to the Moses 2005A vertical profile in Jupiter's non-auroral and auroral regions.

Keywords: Atmospheres, chemistry; Aurorae; Infrared observations; Jupiter, atmosphere; Jupiter, magnetosphere

1. Introduction

The polar stratosphere of Jupiter is coupled to the external magnetospheric environment. High-energy ions and electrons from the jovian magnetosphere and solar wind are injected into the neutral atmosphere and deposit their energy at pressures as deep as the 1-mbar level (Flasar et al. 2004, or approximately 175 km above the 1-bar level). The resulting charged particle precipitation, ion drag and Joule heating exemplify processes that warm the stratosphere and mesosphere, thereby enhancing the mid-infrared emission features of stratospheric species such as CH_4 (methane), C_2H_2 (acetylene),C_2H_4 (ethylene) and C_2H_6 (Caldwell et al., 1980, 1983; Kim et al., 1985; Kostiuk et al., 1993; Livengood et al., 1993; Drossart et al., 1993). The increased flux of electrons in the auroral regions also drives increased rates of ion-neutral and electron-recombination reactions, thereby modifying the chemistry in the auroral regions with respect to non-auroral regions and lower latitudes (Sinclair et al., 2017a, 2018).

Our goal is to better understand and quantify this phenomenon using previous spacecraft and Earth-based spectroscopic measurements. In Sinclair et al. (2017a), henceforth 'Paper I', we performed a retrieval analysis of $\Delta\tilde{\nu}$ = 4.3 cm^{-1} Voyager-1-IRIS (Infrared Interferometer Spectrometer and Radiometer, Hanel et al. 1980) spectra obtained in November

*Corresponding Author
Email address: james.sinclair@jpl.nasa.gov (J. A. Sinclair)

1979 and $\Delta\tilde{\nu}$ = 0.25-2.5 cm^{-1} Cassini-CIRS (Composite Infrared Spectrometer, Kunde et al. 1996) spectra obtained in January 2001. Spectra were inverted using NEMESIS (a forward model and retrieval code, Irwin et al. 2008) to derive the three-dimensional (latitude, longitude, altitude) distributions of stratospheric temperature, C_2H_2 and C_2H_6 at Jupiter's high latitudes. In Sinclair et al. (2018), we performed a similar analysis of IRTF-TEXES (Texas Echelon Cross Echelle Spectrograph, Lacy et al. 2002, on NASA's Infrared Telescope Facility). Both datasets reveal the thermal structure to be vertically bifurcated in Jupiter's auroral regions with warmer temperatures at pressures of approximately 1 mbar and 10 μbar with respect to non-auroral regions. The heating at 10 μbar (or approximately 275 km above the 1-bar level) is near-coincident horizontally and in altitude with Jupiter's diffuse ultraviolet, auroral emission, which is inferred to be driven by lateral Pedersen currents (e.g. Badman et al. 2015; Gladstone et al. 2017). Thus, the 10-μbar heating is likely to be driven by Joule heating associated with these currents. The source of 1-mbar heating is less certain although we have suggested different hypotheses in recent work. One hypothesis was direct precipitation of energetic particles: preliminary particle precipitation depth modeling shows 1.7 MeV e^- or 30 MeV protons precipitate to this pressure level (Ozak et al., 2010; Houston et al., 2018). Our second hypothesis is the production of photochemical haze particles by ion-chemistry, which are then heated by shortwave solar radiation and perhaps downward shortwave auroral emission from higher altitudes. Such haze particles were detected at Jupiter's poles during the Cassini flyby (West et al., 2003) and are present also at the poles of Saturn (Guerlet et al., 2015; Koskinen et al., 2016).

In terms of the chemistry, our analysis of Voyager-IRIS and Cassini-CIRS observations indicated that C_2H_2 was enriched in Jupiter's auroral regions with respect to non-auroral regions in the same latitude band. However, C_2H_6 exhibited negligible change (within measurement uncertainty) or even a decrease in abundance in Jupiter's auroral regions with respect to non-auroral regions. Our analysis of IRTF-TEXES measurements showed similar results and also demonstrated that C_2H_4, like C_2H_2, was enriched in Jupiter's auroral regions. The increase in C_2 hydrocarbon abundances from auroral activity is predicted in the Wong et al. 2000 and Wong et al. 2003 coupled ion-neutral chemistry models for Jovian auroral regions, but little quantitative information was provided. We therefore formed a working interpretation based on neutral photochemical models (e.g., Moses et al. (2000, 2005); Hue et al. (2018) and ion-neutral chemical modeling of Titan's atmosphere (e.g., Wilson and Atreya 2004; Vuitton et al. 2007, 2008; De La Haye et al. 2008; Krasnopolsky 2009). The dominant production pathway of the unsaturated C_2 hydrocarbons is expected to be via electron recombination of the $C_2H_5^+$ ion whereas the dominant production pathway of the C_2H_6 is expected to involve ion-neutral charge exchanges of the $C_2H_5^+$ ion with heavier, neutral hydrocarbons. Detailed discussion of the chemical reactions are provided in Section 6.2 of Paper I as well as Section 5 in this paper. The rate coefficients of the electron recombination reactions that produce the unsaturated C_2 hydrocarbons are expected to be two orders of magnitude greater than the ion-neutral charge-exchange reactions that produce C_2H_6 (Anicich, 2003; Florescu-Mitchell and Mitchell, 2006). Thus, the chemistry in Jupiter's auroral regions would favor the production of C_2H_2 and C_2H_4 in comparison to C_2H_6. Once advected outside the auroral region, neutral photochemistry would dominate over ion chemistry, where C_2H_2 and C_2H_4 would be readily converted into C_2H_6 through sequential H-atom addition (Moses et al., 2000, 2005). Once produced, C_2H_6 has a long lifetime at the 1-mbar level of greater than approximately 100 years (Moses et al., 2005; Hue et al., 2018) and would be advected zonally at high latitudes leading to a zonally-constant abundance with longitude or perhaps an apparent depletion in Jupiter's auroral regions due to its source at non-auroral longitudes. Meridionally, this process would also enrich the zonal-mean C_2H_6 abundance at Jupiter's high latitudes. Equator-to-pole enhancements of C_2H_6 have been observed on both Jupiter (Nixon et al., 2007, 2010; Fletcher et al., 2016; Melin et al., 2018) and Saturn (Howett et al., 2007; Hesman et al., 2009; Guerlet et al., 2009; Sinclair et al., 2013, 2014) in the absence of a similar meridional trend in C_2H_2. This decoupling of C_2H_2 and C_2H_6 has been attributed to large-scale equator-to-pole circulation on timescales longer than the lifetime of C_2H_2 in the lower stratosphere (~100 years at the 1-mbar level, Moses and Greathouse 2005). However, we now also favor the auroral-driven chemistry at high latitudes, as detailed above, as a further source of high-latitude C_2H_6.

In this paper, we seek to derive the abundances of C_2H_4, CH_3C_2H, C_4H_2 and C_6H_6 at Jupiter's high latitudes from Voyager and Cassini in order to test our understanding of how auroral processes modify the stratospheric chemistry. While C_2H_4 can be measured from Earth-based telescopes (e.g. Kostiuk et al. 1993; Sinclair et al. 2018), CH_3C_2H, C_4H_2 and C_6H_6 are a challenge/impossible to measure from Earth since their spectral emission features (at approximately 632, 628 and 674 cm^{-1}, respectively) are heavily obscured by telluric CO_2 absorption. Mid-infrared spectroscopy from the Mid-Infared Instrument (MIRI, Rieke et al. 2015; Glasse et al. 2015) on the James Webb Space Telescope will not offer an immediate solution since its detectors will exhibit a non-linear response to Jupiter's strong thermal emission at these wavelengths (Norwood et al., 2016). Thus, a retrospective analysis of Voyager-IRIS and Cassini-CIRS spectra acquired during the spacecrafts' respective flybys of Jupiter are one of the only means to constrain the abundances of these species in the lower stratosphere from a consistent dataset. We therefore performed a forward-model analysis of Voyager-IRIS and Cassini-CIRS observations obtained in November 1979 and January 2001 in order to derive the abundances of the targeted minor hydrocarbons.

Coadd Name	Min. Latitude (°)	Max. Latitude (°)	Min. Longitude (°)	Max. Longitude (°)	Min. emission angle (°)	Max. emission angle (°)	Number of spectra	Number of deep-space spectra
MIRMAP-NA (Paper I)	67.5	72.5	170.0	190.0	69.6	74.8	6	33
MIRMAP-NQ (Paper I)	67.5	72.5	50.0	70.0	69.8	73.4	11	35
MIRMAP-NA2 (This work)	60.0	80.0	150.0	210.0	61.4	78.3	186	295
MIRMAP-NQ2 (This work)	60.0	80.0	210	150	60.9	78.7	1065	337

Table 1: Details of the MIRMAP-NA and MIRMAP-NQ coadded spectra from Paper I and the updated spectra, named 'MIRMAP-NA2', 'MIRMAP-NQ2' spectra adopted in this paper. All latitudes are planetographic and longitudes are System III West.

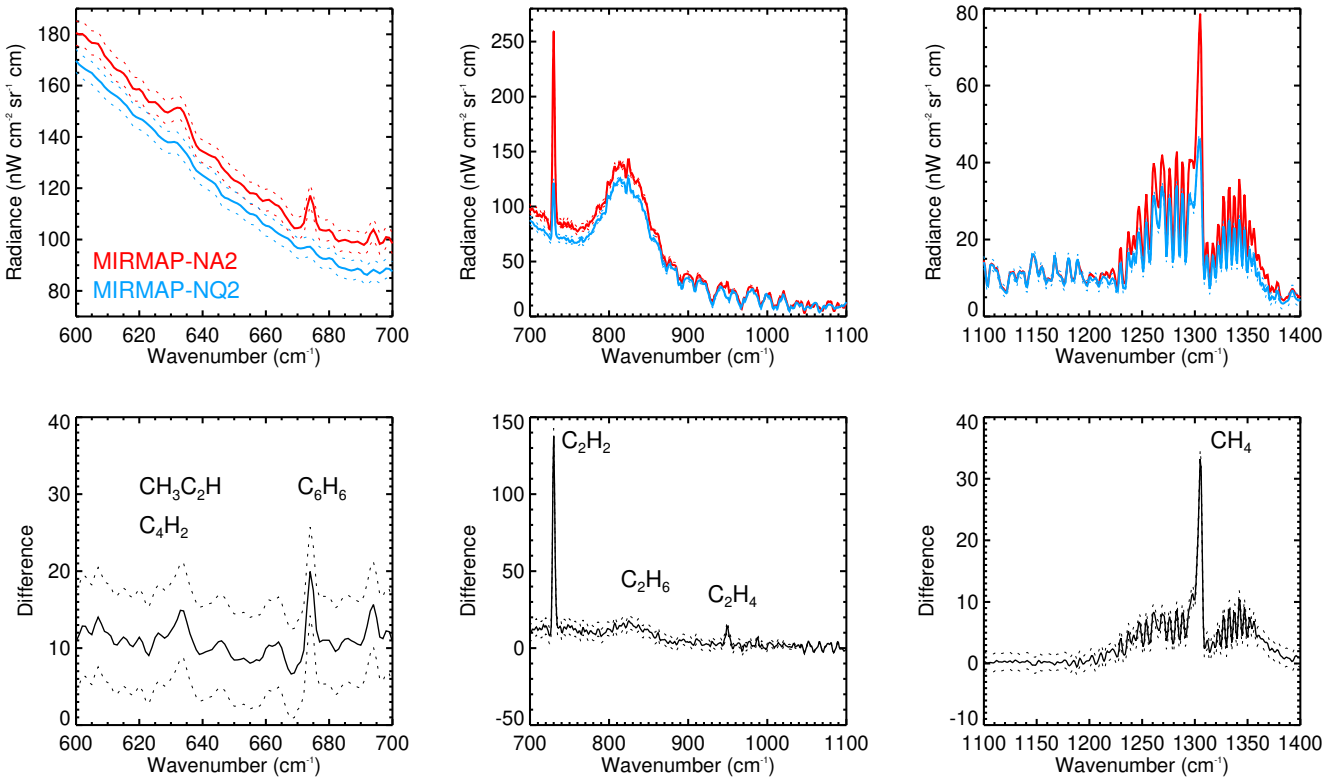

Figure 1: The top row shows the MIRMAP-NA2 (red) and MIRMAP-NQ2 (blue) coadded spectra (solid), which respectively represent an auroral and quiescent region at Jupiter's high-northern latitudes. 1-σ noise levels are shown as dotted lines of the same color. The bottom row shows the residual between the MIRMAP-NA2 and MIRMAP-NQ2 spectra (solid) and uncertainty (dotted, computed by adding the noise on the spectra in quadrature). Spectra and residual spectra are shown over three wavenumber ranges, which capture the spectral emission of the target minor species, as well as CH_4, C_2H_2 and C_2H_6.

2. Observations

Details of the Voyager-IRIS (Hanel et al., 1980) and Cassini-CIRS (Kunde et al., 1996) observations are provided at greater length in Paper I (Sinclair et al., 2017a). Individual spectra were coadded in order to improve the effective signal-to-noise ratio. Spatial averages were performed over latitude and longitude ranges capturing the northern and southern auroral regions and non-auroral regions in the same latitude band for comparison. In paper I and in this paper, the spectra are labelled using the format 'DATASET-XY', where 'DATASET' refers to the spectral dataset - Voyager, 'MIRMAP' (Cassini-CIRS $\Delta\tilde{\nu}$ = 2.5 cm^{-1}) or 'COMPSIT' (Cassini-CIRS $\Delta\tilde{\nu}$ = 0.5 cm^{-1}), X denotes the hemisphere 'N' or 'S', and Y indicates whether the spatial average covers the auroral region, 'A' or a non-auroral, quiescent region, 'Q'. The Voyager-NA, Voyager-NQ, COMPSIT-NA, COMPSIT-NQ, COMPSIT-SA and COMPSIT-SQ spectra analysed in this paper are identical to those presented in Paper I. These spectra are shown in Figures A.9 and A.10 for reference.

The coaddition of CIRS 2.5 cm^{-1} MIRMAP spectra differed from the spectra presented in Paper I. Cassini-CIRS recorded four sets of 2.5 cm^{-1} spectra during its 2001

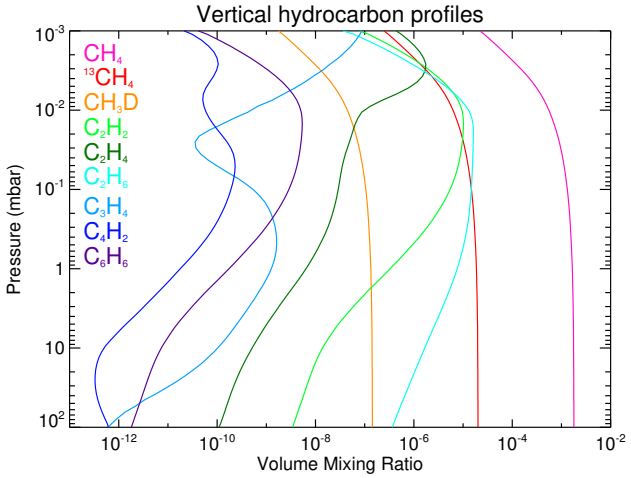

Figure 2: The model vertical profiles of hydrocarbons adopted in this study, colored according to the legend. The vertical profiles of CH_4 and its isotopologues were taken from Romani (1996) while the vertical profiles of all other hydrocarbons were taken from Moses 2005A at 30°N.

flyby - 'ATMOS02A', 'ATMOS02B', 'ATMOS02C' and 'ATMOS02D' - which were acquired between January 1st and January 11th 2001. In Paper I, we used only ATMOS02A spectra whereas in this paper, we coadded all four datasets in order to increase the number of individual target spectra available for coaddition and therefore increase the effective signal-to-noise ratio. We note that the mid-infrared auroral emission has been observed to vary on timescales of days in previous studies (e.g. Kostiuk et al. 1993; Livengood et al. 1993; Sinclair et al. 2017). The spectra recorded of the northern auroral region from the ATMOS02A, B, C and D datasets are in agreement within the 1-σ noise level with exception of the C_2H_2 emission feature at ~730 cm^{-1} (see Figure B.12). Thus, the average of all ATMOS02A, B, C and D datasets represents a temporal average between January 1st and 11th 2001. In a further attempt to increase the number of individual target spectra, deep-space spectra and therefore increase the effective signal-to-noise ratio, the spectra from ATMOS02A, B, C and D were averaged over larger ranges in latitude and longitude. Table 1 compares details of the 'MIRMAP-NQ' and 'MIRMAP-NA' coadded spectra from Paper I and the coadded spectra adopted in this paper, henceforth named 'MIRMAP-NQ2' and 'MIRMAP-NA2'. Figure 1 shows the MIRMAP-NQ2 and MIRMAP-NA2 spectra and their residual, which highlights the enhanced emission of CH_4, C_2H_2, C_2H_4, CH_3C_2H and C_6H_6 from Jupiter's northern auroral region.

3. Radiative transfer modelling

3.1. Forward model

As in Paper I, radiative transfer forward modelling was conducted using NEMESIS (Irwin et al., 2008) and the correlated-k method (Lacis and Oinas, 1991) for computational efficiency. Spectroscopic line information of CH_4, $^{13}CH_4$, CH_3D, NH_3, PH_3, C_2H_2 and C_2H_6 was adopted from the sources shown in Table 4 of Fletcher et al. (2012). C_2H_4 spectroscopic line information was taken from the GEISA 2003 line database (Jacquinet-Husson et al. 2005, with no updates to the C_2H_4 line lists in subsequent GEISA versions) using the line-broadening coefficients and n = 0.73 temperature dependence derived by Bouanich et al. (2003, 2004). Line information of CH_3C_2H, C_4H_2 and C_6H_6 were adopted from GEISA 2009 (Jacquinet-Husson et al., 2011). For CH_3C_2H and C_4H_2, a 0.075 cm^{-1}/atm and 0.1 cm^{-1}/atm broadening half-width were respectively adopted for each species. For C_6H_6, the broadening half-width assumed a linear-fit to the nitrogen-broadening of Waschull et al. (1998). Temperature dependencies of n = 0.5 for CH_3C_2H and n = 0.75 for C_4H_2 and C_6H_6 were assumed. These line database sources, broadening coefficients and temperarture dependencies were chosen for consistency with other studies using Cassini-CIRS spectra (e.g. Fletcher et al. 2018)). For all the aforementioned gases, three sets of k-distributions were computed at resolutions of 0.5 cm^{-1}, 2.5 cm^{-1} and 4.3 cm^{-1} for modelling the Cassini-CIRS COMPSIT, MIRMAP and Voyager-IRIS spectra of these resolutions respectively. For all k-distributions, a Hamming line function was adopted.

3.2. Model Atmosphere

Details of the model atmosphere are provided in greater detail in Paper I. In summary, the vertical profiles of CH_4 and its isotopologues are taken from a photochemical model by Romani (1996) but with a 5% increase in deep concentrations to match Galileo results (Niemann et al., 1998). This was done for consistency with other studies by the Cassini-CIRS science team who also used these vertical profiles. The vertical profiles of all other hydrocarbons, except C_6H_6, were taken from model A of Moses et al. (2005), which we abbreviate to 'Moses 2005A'. This model did not include ion sources for C_6H_6 in the upper stratosphere, which resulted in the vertical profile of its concentration peaking in the 10- to 1- mbar range, whereas its peak is likely to be at higher altitudes. Instead, we adopted the vertical profile of C_2H_2 from Model A, scaled this profile by a factor of 5.28 x 10^{-4} such that the scaled, 5-mbar volume mixing ratio matched that of the nominal C_6H_6 profile from model A, and adopted this profile as the C_6H_6 vertical profile. Figure 2 shows the vertical profiles of hydrocarbons that are adopted in this study.

3.3. Temperature, C_2H_2, C_2H_6

For the COMPSIT and Voyager spectral observations, which are unchanged in this paper with respect to Paper I, we adopted the retrieved vertical profiles of temperature, C_2H_2 and C_2H_6 from Sinclair et al. (2017a). These are summarized in Figure A.11 for reference.

We retrieved the vertical profiles of temperature, C_2H_2 and C_2H_6 from the MIRMAP-NA2 and MIRMAP-NQ2 spectra,

which differ in temporal and spatial range compared to spectra of the same resolution analyzed in Paper I (see Section 2). Our retrieval approach was identical to that conducted in Paper I. Temperature, C_2H_2 and C_2H_6 were retrieved simultaneously. For tropospheric temperature, we adopted the 600 - 620 cm^{-1} and 640 - 660 cm^{-1} spectral range, which covers collision-induced absorption from 600 - 700 cm^{-1} whilst avoiding the spectral features of C_4H_2, CH_3C_2H and C_6H_6 at approximately 630 cm^{-1} and 674 cm^{-1}. For stratospheric temperature, we adopted the 1230 - 1380 cm^{-1} spectral range of the CH_4 ν_4 emission. C_2H_2 and C_2H_6 were retrieved from their respective emission features at 710 - 750 cm^{-1} and 770 - 890 cm^{-1}. Figure B.13 shows the model-observed spectra comparisons and the retrieved vertical profiles of temperature, C_2H_2 and C_2H_6.

The retrieved results are qualitatively consistent with those retrieved from the MIRMAP-NA/NQ spectra in Paper I, the COMPSIT-SQ, -SA, -NQ and -NA results shown in Figure A.11 and IRTF-TEXES results presented in Sinclair et al. (2018). In comparing the vertical temperature profile between auroral and non-auroral regions, temperatures are predominantly enhanced at 1 mbar and 10 μbar with relatively cooler temperatures at the intermediate level of 0.1 mbar. At the 5-mbar level, C_2H_2 is enhanced in the auroral regions, whereas, C_2H_6 is depleted in auroral regions. Quantitative differences between datasets are attributed to the difference in latitude and longitude range adopted in the spatial coaddition as well as the spectral resolution and therefore vertical sensitivity in the atmosphere.

3.4. Vertical sensitivity

The vertical functional derivatives (dR_ν/dX_i, where R is the radiance at wavenumber, ν and X_i is temperature or abundance at the i^{th} pressure level) were calculated with respect to C_2H_4, CH_3C_2H, C_4H_2 and C_6H_6 at $\Delta\nu$ = 2.5 cm^{-1} spectral resolution. These essentially describe the relative contribution of each atmospheric level to the total observed radiance at the top of atmosphere (see Irwin et al. (2008) and Conrath et al. (1998) for further details). We note the range in spectral resolutions of spectra in this study (0.5 cm^{-1} to 4.3 cm^{-1}) and that the shape and magnitude of vertical functional derivatives depends on the spectral resolution. However, for the sake of brevity, we present only the calculations at $\Delta\nu$ = 2.5 cm^{-1}. The functional derivatives were calculated twice: 1) using the retrieved temperature results outside Jupiter's auroral region (from observation MIRMAP-NQ2, Figure B.13) and 2) using retrieved temperature results inside Jupiter's auroral region (from observation MIRMAP-NA2) to determine whether the vertical sensitivity differed between these two regions.

Figure 3 shows the vertical functional derivatives with respect to C_2H_4, CH_3C_2H, C_4H_2 and C_6H_6. For comparison, the vertical functional derivatives with respect to temperature in the CH_4 ν_4 band, which we use to retrieve the vertical temperature profile, are also shown. At 2.5 cm^{-1}, temperature retrievals are constrained between approximately 20 and 0.5 mbar. In Jupiter's auroral regions, there is sensitivity to temperatures at pressures as high as the 10-μbar level due to the presence of upper-stratospheric heating at this altitude (Sinclair et al., 2017a,b, 2018). Spectral emission lines of C_2H_4 at approximately 950 cm^{-1} predominantly sound the 10- to 0.1-mbar pressure range with a secondary peak in sensitivity at the 5-μbar level. The magnitude of this secondary peak is larger in the auroral region, due to the warmer atmospheric temperatures and line-forming region at this altitude. The spectral emission feature of CH_3C_2H, centered at approximately 632 cm^{-1}, sounds the 10- to 0.1-mbar range while the C_4H_2 emission feature, centered at approximately 628 cm^{-1}, sounds lower pressures from approximately 5- to 0.05-mbar. The spectral emission features of CH_3C_2H and C_4H_2 overlap in spectral range and thus the derivations of their abundances were conducted simultaneously. However, there is significantly less sensitivity to C_4H_2 compared to CH_3C_2H due to the former's lower abundance and line strength and as demonstrated in Section 4, we were only able to derive upper limits on C_4H_2. The spectral emission feature of C_6H_6 at approximately 674 cm^{-1} sounds the 10-mbar to 10-μbar range. In general, the observations are sensitive to C_2H_4, CH_3C_2H, C_4H_2 and C_6H_6 over a pressure range in which there is sensitivity to temperature in the CH_4 ν_4 band, which allows the contributing effects of temperature of the line forming region and abundance on the observed line strength to be disentangled. The exception is the cores of the C_2H_4 emission lines, which sound the 5-μbar level, where there is less sensitivity to temperature. We have attempted to derive abundances of C_2H_4 regardless but readers should note abundances of C_2H_4 may be offset for this reason.

4. Analysis

4.1. Deriving upper-limit abundances in non-auroral regions

The spectra covering high-latitude, non-auroral regions (MIRMAP-NQ2, COMPSIT-SQ, COMPSIT-NQ and Voyager-NQ) were either absent of the spectral features of C_2H_4, CH_3C_2H, C_4H_2 and C_6H_6 and/or any observed spectral features were within the 1-σ noise level. Thus, we derived an upper limit on the abundance of these hydrocarbons.

The upper limit was derived from all four spectra in the same way. The retrieved temperature, C_2H_2 and C_2H_6 vertical profiles (Section 3.3) were adopted. For C_2H_4, CH_3C_2H, C_4H_2 and C_6H_6 in turn, the Moses 2005A modelled vertical profile at 30°N (Figure 2) was scaled by a constant at all altitudes and a forward-model spectrum was calculated at the appropriate emission angle and spectral resolution. The scale factor was increased until the forward-modelled emission feature of the hydrocarbon in question reached the 1-σ upper noise level of the observed spectrum. At this point, the scaled abundance was deemed to represent the 1-σ upper limit abundance. Figure 4 shows the observed spectra in the non-auroral regions, the spectra corresponding to the Moses 2005A predicted vertical

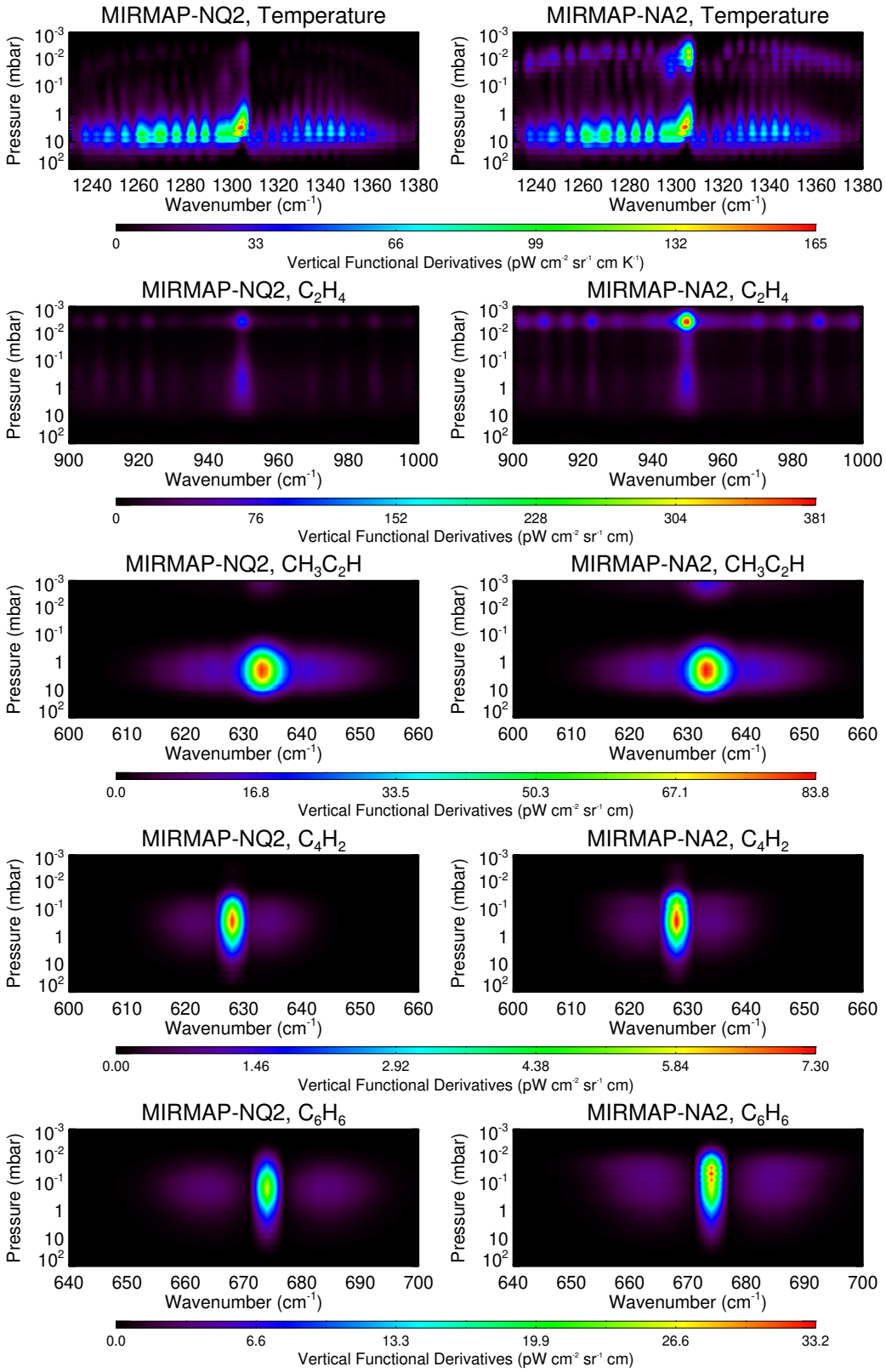

Figure 3: Vertical functional derivatives with respect to temperature (top row), C_2H_4 (2nd row), CH_3C_2H (3rd row), C_4H_2 (4th row) and C_6H_6 (bottom row). The left and right columns show the calculations assuming the retrieved temperature outside the auroral region (from observation MIRMAP-NQ2) and inside the auroral region (MIRMAP-NA2) respectively. These were calculated at $\Delta\tilde{\nu} = 2.5$ cm^{-1} spectral resolution.

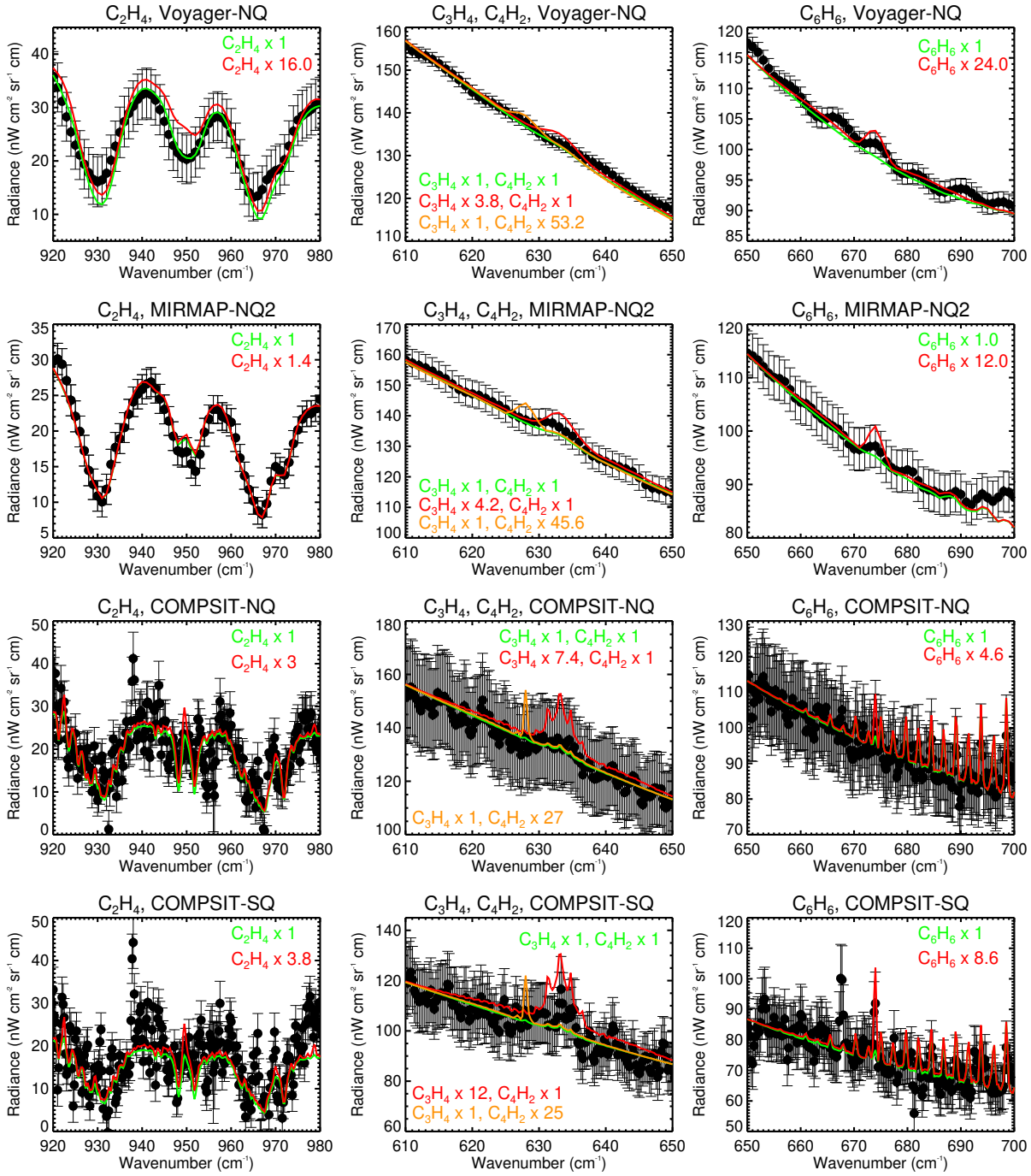

Figure 4: The observed Voyager-NQ (top), MIRMAP-NQ2 (2nd), COMPSIT-NQ (3rd) and COMPSIT-SQ (4th) quiescent observed spectra (black circles with error bars). Solid lines show forward-modelled spectra, where a scale factor was applied to the Moses 2005A hydrocarbon vertical profile as indicated in the legend. In general, green spectra correspond to the Moses 2005A vertical profiles predicted at 30°N, red or orange spectra correspond to the 1-σ upper-limit abundance. Outlier features at ~938 cm^{-1} in theCOMPSIT spectra are considered an instrument artefact. The outlier feature at ~668 cm^{-1} in the COMPSIT-SQ spectrum results from CO_2, which was not the focus of this study. In the legend, CH_3C_2H is shortened to 'C_3H_4'.

profile of abundance and the spectrum corresponding to the 1-σ upper-limit abundance. These results and the corresponding abundances at the 1-mbar level are also summarized in Table 2 in Section 5.

4.2. Deriving concentrations of C_2H_4 and C_6H_6 in auroral regions

The abundances of C_2H_4 and C_6H_6 were derived from all four datasets in the same way. The retrieved temperature, C_2H_2 and C_2H_6 vertical profiles (Section 3.3) were adopted. A

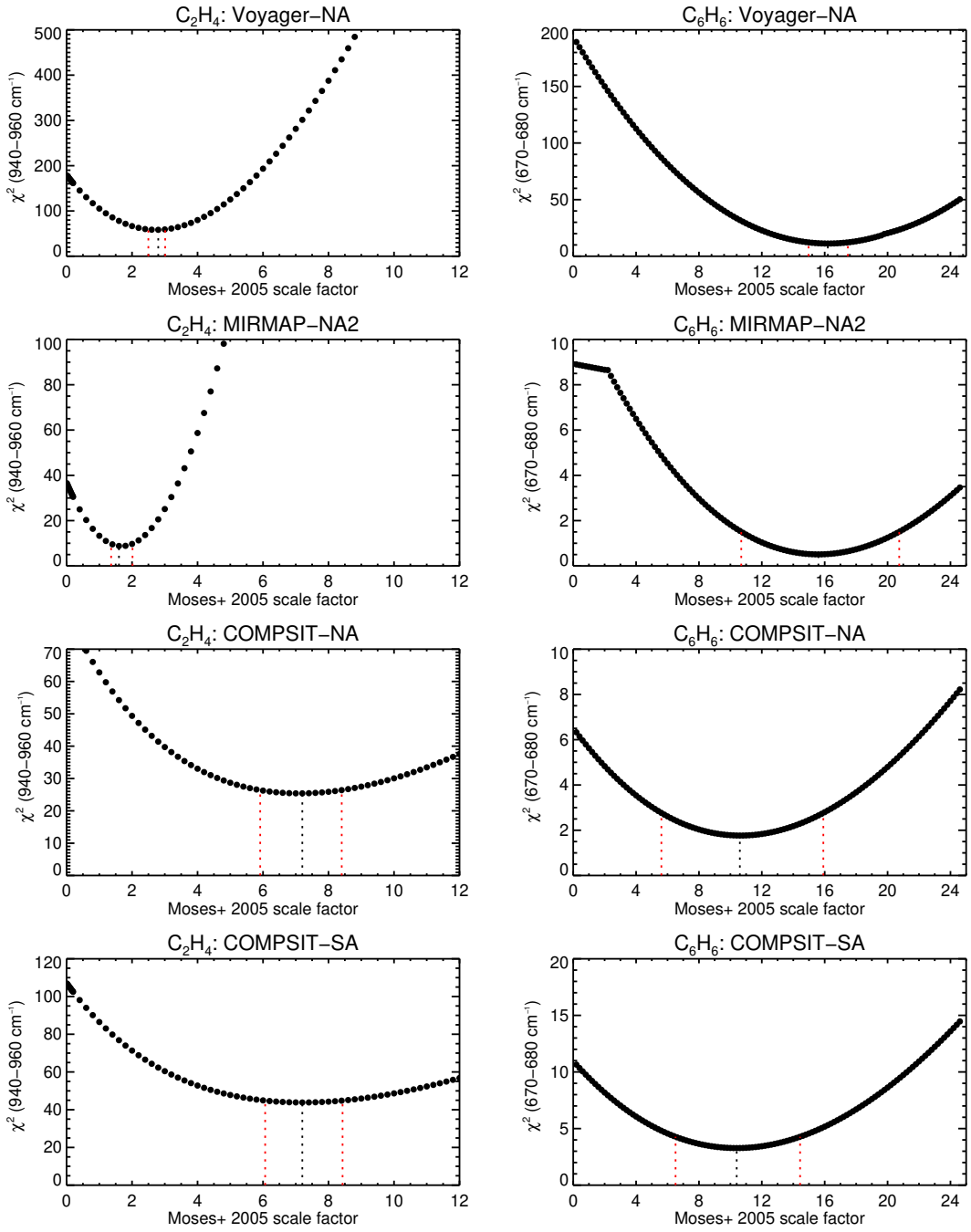

Figure 5: The χ^2 (Equation 1) values (black circles) in the 940 - 960 cm^{-1} spectral range (left) as a function of the scale factor applied to the Moses 2005A predicted vertical profile of C_2H_4 and in the 670.- 680 cm^{-1} spectral range (right) as a function of the scale factor applied to the reference vertical profile of C_6H_6. Results are shown for the Voyager-NA (1st row), MIRMAP-NA2 (2nd row), COMPSIT-NA (3rd row) and COMPSIT-SA (bottom row). The vertical, dashed, black lines below the χ^2 values mark the position of the best-fitting scale factor and the vertical, dashed, red lines mark the corresponding 1-σ confidence level.

scale factor ranging from 0.2 to 30.0 in increments of 0.2 was applied to all altitudes of the reference vertical profile of C_2H_4 (Moses et al. 2005, model A) and a forward-model spectrum was computed in the 900 - 1000 cm^{-1} spectral range at the same emission angle and spectral resolution as the observed spectra. For all forward-modelled spectra, the χ^2 statistic (Equation 1) was computed for the 940 - 960 cm^{-1} range.

$$\chi^2 = \sum_j^N \left(\frac{O_j - M_j}{\sigma_j} \right)^2 \quad (1)$$

O_j, M_j and σ_j are respectively the observed spectral radiance, forward-modelled spectral radiance and noise/uncertainty on

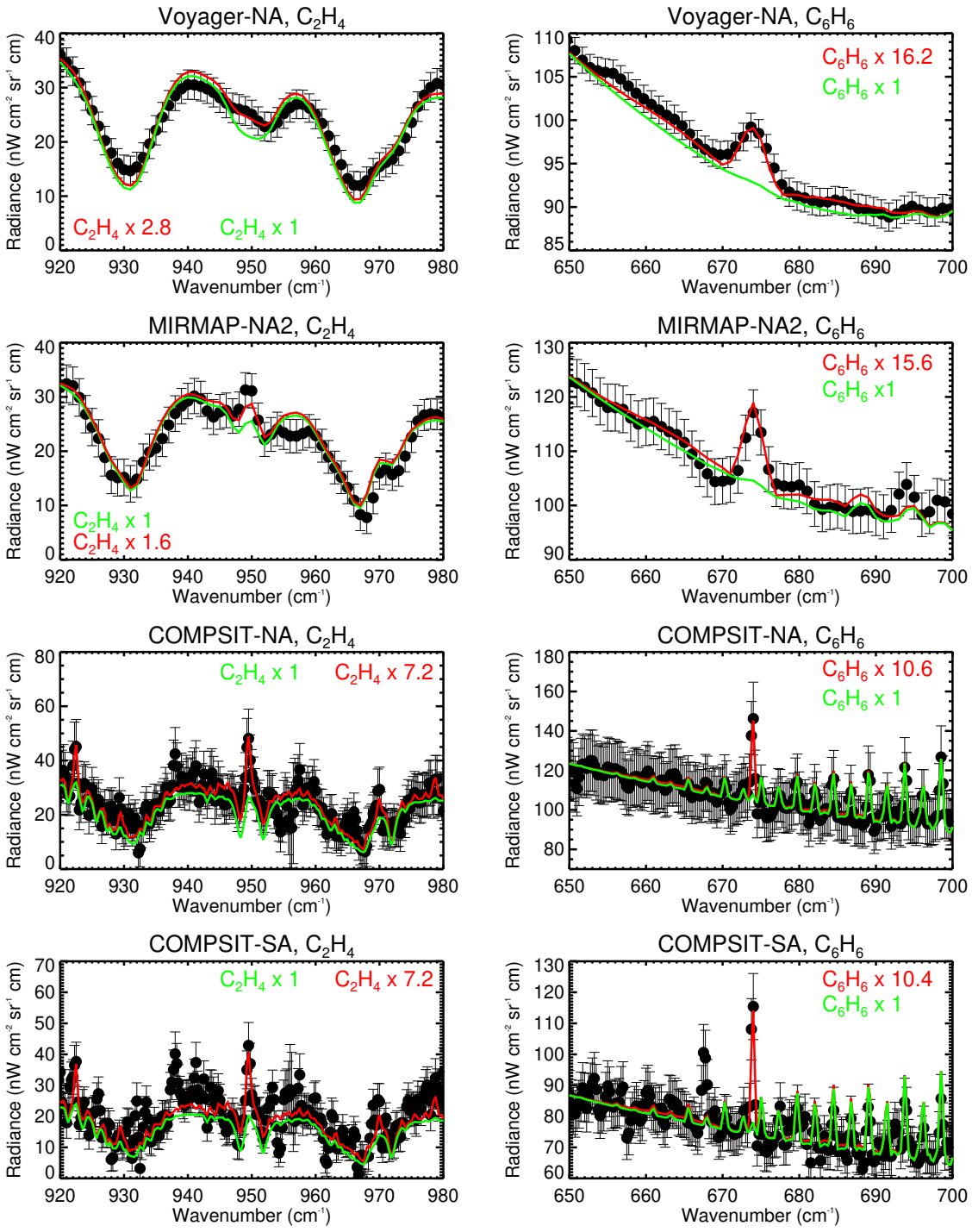

Figure 6: Observed vs. model spectral comparisons for the Voyager-NA (top row), MIRMAP-NA2 (2nd row), COMPSIT-NA (3rd row) and COMPSIT-SA (4th row) in the 920 - 980 cm^{-1} (left column) and 650 - 700 cm^{-1} (right column) range. These spectral ranges target C_2H_4 and C_6H_6 emission respectively. Observed spectra are shown as points with error bars, solid, green spectra correspond to a forward model assuming the reference vertical profile of C_2H_4 or C_6H_6 and red spectra correspond to a scaling of the vertical profile that minimized χ^2 as described in the text and shown in Figure 5.

the observed radiance at wavenumber, j and N is the number of independent spectral points. The scaled vertical profile of C_2H_4 that minimised the χ^2 value, χ^2_{min}, was deemed to represent the best-fitting abundance of C_2H_4. The scaled vertical profile of C_2H_4 that corresponded to χ^2_{min} + 1 was assumed as the 1-σ confidence level on the best-fitting abundance (Press et al., 1992).

The same procedure was performed to determine the best-fitting abundances of C_6H_6 except forward-model spectra were

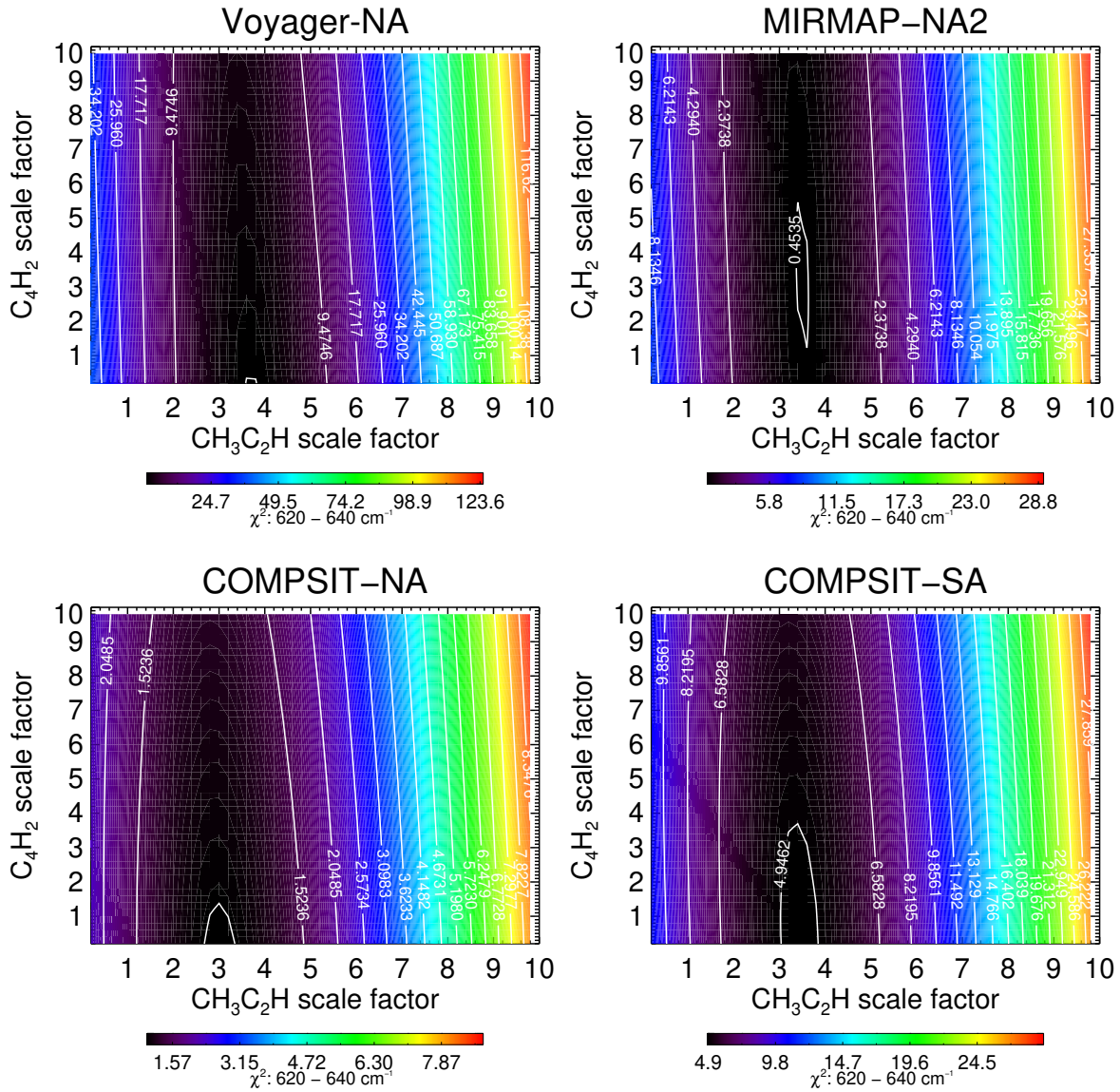

Figure 7: χ^2 distributions with respect to the scale factors applied to the vertical profiles of CH_3C_2H and C_4H_2 from Moses 2005A. Results are shown for the Voyager-NA (top-left), MIRMAP-NA2 (top-right), COMPSIT-NA (bottom-left) and COMPSIT-SA (bottom-right) observations.

computed in the 600 - 700 cm^{-1} spectral range and the χ^2 statistic was calculated from 670 - 680 cm^{-1}. Figure 5 shows the variation in χ^2 as a function of the scale factor applied to the vertical profiles of C_2H_4 and C_6H_6. Figure 6 shows the observed spectra and the modelled spectra that minimised the χ^2 value. The best-fitting abundances and uncertainties are also detailed in Table 2 in Section 5.

4.3. Deriving CH_3C_2H and C_4H_2 abundances in Jupiter's auroral regions

The concentrations of CH_3C_2H and C_4H_2 were determined simultaneously given the proximity of their spectral features (e.g. Figures 3, 4). Initially, the retrieved vertical profiles of temperature, C_2H_2 and C_2H_6 were adopted. A 2-dimensional grid of scale factors applied to the vertical profiles of CH_3C_2H and C_4H_2, from 0.2 to 10.0 in increments of 0.2, were computed. For each combination of CH_3C_2H and C_4H_2 abundance, a forward-model spectrum was computed in the 600 - 700 cm^{-1} and the χ^2 value (Equation 1) was computed in the 620 - 640 cm^{-1} spectral range. The combination of scale factors applied to the vertical profiles of CH_3C_2H and C_4H_2 that minimised χ^2 were considered to be the best-fitting abundances for both species. The 1-σ confidence levels of these best-fitting abundances were determined by finding the scale factors of the CH_3C_2H and C_4H_2 vertical profiles, which corresponded to χ^2_{min}+2.30 (Press et al., 1992).

Figure 7 shows the distributions of χ^2 as a function of the scale factors applied to the vertical profiles of CH_3C_2H and C_4H_2 from Moses 2005A. While there is an evident variation in the value of χ^2 with respect to the abundance of CH_3C_2H, there is

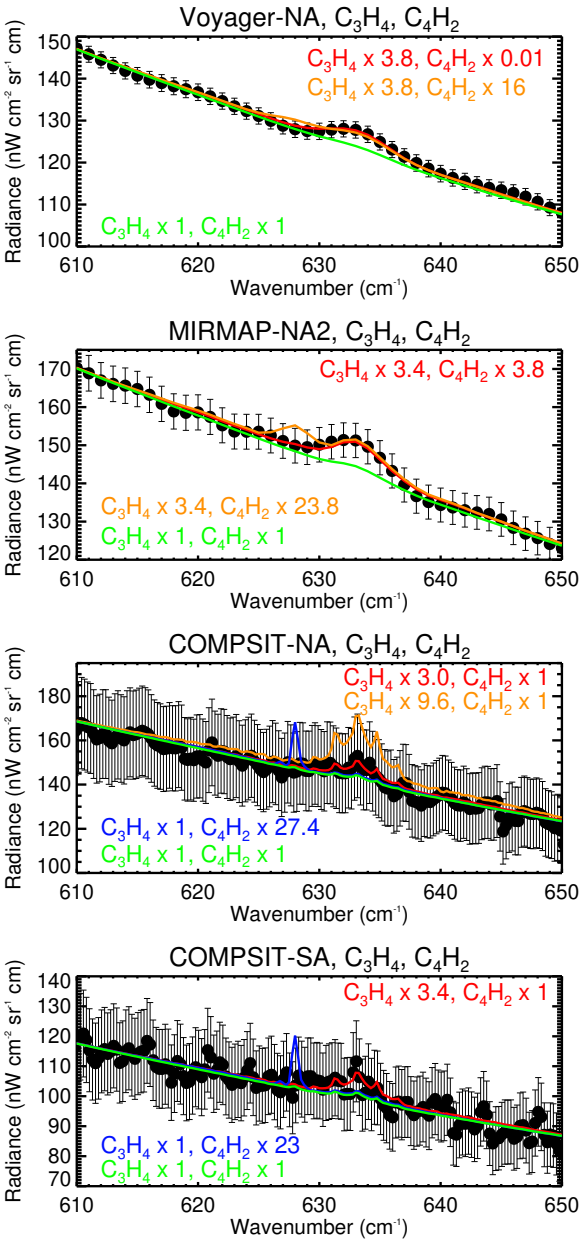

Figure 8: The observed Voyager-NA (top panel), MIRMAP-NA2 (2nd panel), COMPSIT-NA (3rd panel) and COMPSIT-SA (4th panel) spectra in the 610 - 650 cm^{-1} spectral range. Solid, colored lines show forward model spectra with abundances of CH_3C_2H and C_4H_2 relative to the Moses 2005A vertical profiles indicated in the legend. In the legend, CH_3C_2H is shortened to 'C_3H_4'.

little to negligible constraint on the abundance of C_4H_2 from the observations. This was deemed a result of its lower abundance, weaker line feature and the limited signal-to-noise ratio of the measurements. Using a similar method as detailed in Section 4.1, we derived a 1-σ upper limit abundance for C_4H_2 ffrom all four datasets of the auroral regions.

The spectra corresponding to the best-fitting abundances of CH_3C_2H and upper limits of C_4H_2 are shown in Figure 8. These results and abundances at the 1-mbar level are also quoted in Table 2. For the Voyager-NA, MIRMAP-NA2 and COMPSIT-SA spectra, the best-fitting abundances of CH_3C_2H were significantly higher (outside the 1-σ confidence level) than the value predicted by Moses 2005A for a lower latitude. However, for the COMPSIT-NA spectrum, there was insufficient constraint on the abundance of CH_3C_2H and thus we derived a 1-σ upper limit on its abundance using a method similar to that described in Section 4.1.

5. Discussion

Table 2 summarizes the abundances of C_2H_4, CH_3C_2H, C_4H_2 and C_6H_6 derived from the Voyager and Cassini spectra. With respect to the predicted abundances from Moses 2005A of a lower latitude, a statistically-significant enrichment of C_2H_4 and C_6H_6 is required for all spectra covering Jupiter's northern and southern auroral regions. This is similarly true for CH_3C_2H with exception of the COMPSIT-NA observation of Jupiter's northern auroral region for which only an upper-limit abundance was derived. The Moses 2005A model values were themselves adjusted in order to match abundances derived from ISO observations of Jupiter's equatorial regions (e.g. Bézard et al. 2001a,b). From photochemistry alone, the zonal-mean meridional distributions of these hydrocarbons would be expected to peak at equatorial latitudes, which receive the most solar radiation, and decrease towards the poles (e.g. Moses et al. 2000, 2005; Hue et al. 2018). Larger-scale equator-to-pole circulation on timescales longer than ~100 years has been suggested in previous studies to explain the equator-to-pole enrichment of C_2H_6 on Jupiter (Nixon et al., 2007, 2010; Melin et al., 2018; Hue et al., 2018) and Saturn (Howett et al., 2007; Hesman et al., 2009; Guerlet et al., 2009; Sinclair et al., 2013, 2014) in the absence of a similar trend in C_2H_2. As discussed in Section 1, we also favor the production of C_2H_6 at high latitudes through auroral chemistry as the explanation for this behavior. Nevertheless, if such an equator-to-pole circulation does exist, the minor hydrocarbons in this study would be insensitive to this long-timescale transport since their chemical lifetimes are considerably shorter than ~100 years at the 1-mbar level (on the order of days to a few Earth years, Moses et al. 2005; Moses and Greathouse 2005; Guerlet et al. 2010, 2015). Thus, the fact that an enrichment of these hydrocarbons exists in Jupiter's auroral regions compared to lower-latitude values is suggestive of a chemical source rather than a dynamical source.

Indeed, a subset of observations show abundances in Jupiter's auroral regions are enriched with respect to upper-limit abundances derived outside the auroral region in the same latitude band. This is highly suggestive of a chemical source localized within Jupiter's auroral region in contrast to meridional advection, which would instead be expected to enhance the zonal mean. For example, 1-mbar C_2H_4 abundances of $46.95^{+10.03}_{-8.14}$ and $46.95^{+8.02}_{-7.40}$ were derived from 0.5 cm^{-1} CIRS observations of Jupiter's northern and southern auroral regions respectively. These are statistically-significant with respect to upper-limit abundances of <19.56 ppbv and <24.78 ppbv derived outside the auroral region in the same

Species	Non-auroral regions			Auroral regions		
	Observation	Scale factor applied to Moses+ 2005 profile	Abundance at 1 mbar (ppbv)	Observation	Scale factor applied to Moses+ 2005 profile	Abundance at 1 mbar (ppbv)
C_2H_4	Voyager-NQ	<16.0	<104.38	Voyager-NA	$2.80^{+0.21}_{-0.30}$	$18.26^{+1.39}_{-1.97}$
	MIRMAP-NQ2	<1.4	<9.13	MIRMAP-NA2	$1.60^{+0.41}_{-0.21}$	$10.44^{+2.70}_{-1.55}$
	COMPSIT-NQ	<3.0	<19.56	COMPSIT-NA	$7.20^{+1.20}_{-1.29}$	$46.95^{+7.85}_{-8.38}$
	COMPSIT-SQ	<3.8	<24.78	COMPSIT-SA	$7.20^{+1.23}_{-1.13}$	$46.95^{+8.01}_{-7.40}$
CH_3C_2H	Voyager-NQ	<3.8	<4.86	Voyager-NA	$3.80^{+0.78}_{-0.96}$	$4.86^{+0.25}_{-0.48}$
	MIRMAP-NQ2	<4.2	<5.88	MIRMAP-NA2	$3.40^{+1.89}_{-1.69}$	$4.35^{+2.42}_{-2.16}$
	COMPSIT-NQ	<7.4	<9.46	COMPSIT-NA	<9.6	<12.28
	COMPSIT-SQ	<12.0	<15.35	COMPSIT-SA	$3.40^{+2.06}_{-1.94}$	$4.35^{+2.63}_{-2.48}$
C_4H_2	Voyager-NQ	<53.2	<0.972	Voyager-NA	<16.0	<0.29
	MIRMAP-NQ2	<45.6	<0.833	MIRMAP-NA2	<23.8	<0.43
	COMPSIT-NQ	<27.0	<0.493	COMPSIT-NA	<27.4	<0.50
	COMPSIT-SQ	<25.0	<0.457	COMPSIT-SA	<23.0	<0.42
C_6H_6	Voyager-NQ	<24.0	<4.31	Voyager-NA	$16.20^{+1.27}_{-1.23}$	$2.91^{+0.23}_{-0.22}$
	MIRMAP-NQ2	<12.0	<2.15	MIRMAP-NA2	$15.60^{+5.14}_{-4.90}$	$2.80^{+0.92}_{-0.88}$
	COMPSIT-NQ	<4.6	<0.83	COMPSIT-NA	$10.60^{+5.31}_{-4.99}$	$1.90^{+0.95}_{-0.90}$
	COMPSIT-SQ	<8.6	<1.54	COMPSIT-SA	$10.40^{+4.04}_{-3.89}$	$1.87^{+0.72}_{-0.70}$

Table 2: Derived scaled factors with respect to the Moses et al. 2005 model A vertical profiles of C_2H_4, CH_3C_2H, C_4H_2 and C_6H_6 and the corresponding abundance at the 1-mbar level. Results for non-auroral regions and auroral regions are shown in the left- and right-hand columns respectively. Values preceded with a '<' denote the quoted abundance is a 1-σ upper limit. Differences in derived abundances between the datasets are attributed to differences in the spatial ranges adopted in the coaddition of spectra, the spectral resolution and temporal variability.

latitude band from the same dataset. A statistically-signfiicant enrichment of C_6H_6 in Jupiter's northern auroral region with respect to the zonal mean outside the auroral region is also true in comparing abundances derived from the 0.5 cm^{-1} CIRS observations. However, for the remaining results, derived abundances of C_2H_4, CH_3C_2H and C_6H_6 in Jupiter's northern and southern auroral regions are not statistically significant with respect to the upper-limit abundances derived in the same latitude band outside the auroral region. This may simply be a result of the lack of sensitivity in observations in non-auroral regions rather than there being little contrast in abundance between auroral and non-auroral regions. Stratospheric temperatures are cooler in Jupiter's non-auroral regions, which yields less thermal emission from the line-forming altitudes. This results in a lower signal-to-noise ratio, which is augmented by a lack of individual spectra at high latitudes due to the near-equatorial orbits of both Voyager and Cassini spacecraft as they made their Jupiter flybys.

With respect to the modelled value at 30°N (Moses et al., 2005), C_2H_4 is enriched in both Jupiter's northern and southern auroral regions. For example, from CIRS 2.5 cm^{-1} (MIRMAP-NA2) observations of the northern auroral region, we derived an abundance of $10.44^{+2.70}_{-1.55}$ ppbv at the 1-mbar level, which represents an approximate 60% increase with respect to the modelled values at the same pressure level and abundances derived by Morrissey et al. (1995) and Bézard et al. 2001a. At the 1-mbar level, Sinclair et al. (2018) derived an abundance of 6.509 ± 0.811 ppbv at 70°N 180°W (the center of the northern auroral region) from a retrieval analysis of IRTF-TEXES observations measured in December 2014. This is in disagreement outside the 1-σ confidence level of the value derived in this work but is at least comparable in order of magnitude. We attribute the different abundances between the two studies to: 1) potential temporal variability between observations in 1979 and 2001 (this work) and 2014 (Sinclair et al., 2018) and 2) the differing spectral resolutions of the datasets used ($\Delta\tilde{\nu} > 0.25$ cm^{-1} in this study and $\Delta\tilde{\nu} <$ 0.015 cm^{-1} in Sinclair et al. (2018)), which result in different vertical sensitivities in the atmosphere. At the 10-µbar level, Kostiuk et al. (1993) derived a C_2H_4 abundance of <2 ppmv at equatorial latitudes and high-northern latitudes outside the auroral region and an 18-fold enrichment (~36 ppmv) within the northern auroral region. While our derived upper-limit abundances of C_2H_4 outside the auroral region are comparable

with these values, our derived abundances of C_2H_4 in the northern auroral region are over an order of magnitude lower than those derived by Kostiuk et al. (1993). Again, we attribute this discrepancy to possible temporal variability between the Kostiuk et al. (1993) observations measured in 1986 and those of this study as well as contrasts in spectral resolving power.

With exception of the COMPSIT-NA observation, the remaining spectra of Jupiter's auroral regions demonstrate that CH_3C_2H is enriched with respect to modelled values at 30°N. For example, from the MIRMAP-NA2 observation, we derived an abundance of $4.35^{+2.42}_{-2.16}$ ppbv at the 1-mbar level compared to the 1.279 ppbv abundance predicted by Moses 2005A at lower latitudes and column-integrated abundances derived by Fouchet et al. (2000) at low-jovian latitudes. For C_4H_2, we were only able to derive upper-limit abundances for all spectra in both auroral and non-auroral regions.

As discussed in Section 1 and Sinclair et al. (2017a, 2018), we believe the enhanced flux of ions and electrons in Jupiter's auroral regions drives faster reaction rates of ion-related chemistry. By analogy with ion-neutral chemical models of Titan (e.g. De La Haye et al. 2008), we believe the dominant production mechanism for C_2H_4 is by electron-recombination of the $C_2H_5^+$ ion. The $C_2H_5^+$ ion is itself produced through reactions (2)-(4) below.

$$H_2 + e^- \longrightarrow H^+ + H + 2e^- \quad (2)$$
$$H^+ + CH_4 \longrightarrow CH_3^+ + H_2 \quad (3)$$
$$CH_3^+ + CH_4 \longrightarrow C_2H_5^+ + H_2 \quad (4)$$

with e^- representing an electron (either auroral in source or secondary from the interaction of the precipitating particles with atmospheric constituents). Once $C_2H_5^+$ is produced, dissociative recombination of $C_2H_5^+$ with electrons can then produce unsaturated C_2 hydrocarbons, such as C_2H_4, as shown in reactions (5)-(7) below.

$$C_2H_5^+ + e^- \longrightarrow C_2H_2 + H_2 + H \quad (5)$$
$$C_2H_5^+ + e^- \longrightarrow C_2H_2 + 3H \quad (6)$$
$$C_2H_5^+ + e^- \longrightarrow C_2H_4 + H \quad (7)$$

Thus, these reactions would similarly be expected to enrich C_2H_2 in Jupiter's auroral regions with respect to lower-latitude values, which has been observed (Drossart et al., 1993; Sinclair et al., 2017a, 2018). The chemistry of CH_3C_2H and C_4H_2 is expected to be closely linked with that of C_2H_2 (e.g., Moses et al. 2000, 2005). At all latitudes, C_2H_2 photolysis leads to C_2H production, which then reacts with C_2H_2 to form C_4H_2 ($C_2H + C_2H_2 \longrightarrow C_4H_2 + H$). Within the auroral regions, there are additional sources of C_2H through dissociative recombination of $C_2H_2^+$, $C_2H_3^+$, $C_2H_4^+$, $C_3H_2^+$, $C_3H_3^+$, $C_3H_4^+$ and other ions. In fact, the chemistry is non-linear, so that an increase in C_2H_2 would be expected to lead to an even larger increase in CH_3C_2H and C_4H_2. Given the enhanced C_2H_2 abundances derived in the Jovian auroral regions, we would expect an associated and larger increase in the CH_3C_2H and C_4H_2 abundances in Jupiter's auroral region. From the MIRMAP-NA2 observation (Figure B.13), a C_2H_2 abundance of 305.6 ± 29.5 ppbv is retrieved at the 1-mbar level. In Paper I, we derived a similar C_2H_2 abundance of 341.5 ± 73.4 ppbv from similar 2.5 cm^{-1} CIRS spectra coadded over different ranges in date and latitude/longitude (as discussed further in Section 2 of this paper). The C_2H_2 abundance derived in this paper at high latitudes represents a ~19% increase with respect to the C_2H_2 abundance predicted by Moses 2005A and a ~39% increase with respect to C_2H_2 abundances derived from CIRS observations at Jupiter's low latitudes (Nixon et al., 2007). For CH_3C_2H, a larger, 3-4 scale-factor enrichment is required with respect to lower-latitude values to fit its spectral emission feature from the same observation (Table 2). Thus, our derived abundances of C_2H_2 and CH_3C_2H suggest this non-linear relationship might be true. However, we cannot determine whether C_4H_2 follows this relationship since our derived upper-limit abundances are over and order of magnitude higher (Table 2).

C_6H_6 is significantly enriched in both Jupiter's northern and southern auroral regions with respect to lower-latitude values. Scale-factor enrichments of close to or larger than an order of magnitude are required to fit the emission features of C_6H_6 at 674 cm^{-1} in all sets of observations. For example, we derive an abundance of C_6H_6 of $2.80^{+0.92}_{-0.88}$ ppbv at the 1-mbar level from the MIRMAP-NA2 observation. This is a factor of $15.60^{+5.14}_{-4.90}$ larger than the vertical profile predicted by (Moses et al., 2005), which itself reproduced the measured column abundances by Bézard et al. (2001b) at low latitudes. As detailed in Wong et al. (2003), the dominant production of C_6H_6 involves electron recombination of the $C_6H_7^+$ ion (Reaction 10), which is produced below via reactions (8)-(9).

$$C_6H_5^+ + H_2 \longrightarrow C_6H_7^+ \quad (8)$$
$$C_3H_5^+ + C_3H_4 \longrightarrow C_6H_7^+ + H_2 \quad (9)$$
$$C_6H_7^+ + e^- \longrightarrow C_6H_6 + H \quad (10)$$

We note the association reaction $C_4H_3^+ + C_2H_4 \longrightarrow C_6H_7^+$ may also play a role, as on Titan (e.g. De La Haye et al. 2008; Vuitton et al. 2008). Benzene is the primary molecule involved in the formation of polycyclic aromatic hydrocarbons (PAHs), which themselves are the building blocks of haze particles (Wong et al., 2000; Friedson et al., 2002; Wong et al., 2003). These haze particles have been observed at Jupiter's poles (Pryor and Hord, 1991; West et al., 2003) and we believe their absorption of shortwave radiation may be one of the sources of 1-mbar heating that have been inferred from temperature retrievals (see Section 1, Figures A.11 and B.13, Sinclair et al. 2017b, 2018). Benzene was also found to be enriched at Saturn's poles in comparison to equatorial latitudes, which was attributed to ion-related reactions driven by the aurora (Guerlet et al., 2015; Koskinen et al., 2016; Fletcher et al., 2018).

We note to readers a caveat of our analysis, which assumed that the vertical profiles of C_2H_4, CH_3C_2H and C_4H_2 are

unchanged with respect to those derived by the Moses et al. (2005) neutral photochemistry model. We have inferred the presence of ion-related chemistry from enriched abundances at high latitudes. Such ion chemistry could significantly change the shape of the vertical profiles of each species, which in turn would affect abundances derived by a scaling of their vertical profiles. This advocates for further chemical modelling of Jupiter's stratosphere with ion-related chemical reactions in addition to neutral photochemistry to determine how the vertical profiles of observable hydrocarbon species are modified by the aurora.

6. Conclusions

We performed an analysis of $\Delta\tilde{\nu}$ =4.3 cm^{-1} Voyager-1-IRIS and $\Delta\tilde{\nu}$ =0.25-2.5cm^{-1} Cassini-CIRS spectra of Jupiter's high latitudes obtained during the spacecrafts' respective flybys in November 1979 and January 2001. Adopting retrieved results of the vertical temperature, C_2H_2 and C_2H_6 profiles (this paper and (Sinclair et al., 2017a)), spectra were forward-modelled in the 600 - 700 cm^{-1} and 900 - 1000 cm^{-1} spectral range in order to derive the abundances of further minor hydrocarbons: C_2H_4 (ethylene), CH_3C_2H (methylacetylene), C_4H_2 (diacetylene) and C_6H_6 (benzene). With respect to the vertical profiles of these species predicted by a neutral photochemistry model (Moses et al., 2005), a statistically-significant enrichment of C_2H_4, CH_3C_2H and C_6H_6 is required in order to fit the emission features of these hydrocarbons in Voyager-1-IRIS and Cassini-CIRS 2.5 cm^{-1} spectra of Jupiter's northern auroral region and Cassini-CIRS 0.5 cm^{-1} spectra of the southern auroral region. We conclude this provides evidence of enhanced ion-related chemistry in Jupiter's auroral regions due to the signifcantly-enhanced influx of energetic electrons and ions from the jovian magnetosphere and external solar-wind environment. Chemical modelling of Jupiter's stratosphere with the addition of ion-related chemistry and quantification of how the neutral hydrocarbon species are modified would be invaluable in further interpretation of the results presented in this work.

7. Acknowledgements

The research was carried out at the Jet Propulsion Laboratory, California Institute of Technology, under a contract with the National Aeronautics and Space Administration. Many thanks to the NASA Postdoctoral Program (managed by Oak Ridge Associated Universities and then Universities Space Research Association) for funding Sinclair during this research. Fletcher was supported by a Royal Society Fellowship at the University of Leicester. We also thank the Cassini-CIRS team for updating the calibration of CIRS data from the Jupiter flyby. The UK authors thank the Science and Technology Facilities Council (SFTC) for their support. Orton was supported by grants from NASA to the Jet Propulsion Laboratory, California Institute of Technology.

8. References

V. G et al. Anicich. An index of the literature for bimolecular gas phase cation-molecule reaction kinetics. *JPL Publications*, 03(19), 2003. URL `https://trs-new.jpl.nasa.gov/bitstream/handle/2014/7981/03-2964.pdf?sequence=1&isAllowed=y`.

Sarah V. Badman, Graziella Branduardi-Raymont, Marina Galand, Sébastien L. G. Hess, Norbert Krupp, Laurent Lamy, Henrik Melin, and Chihiro Tao. Auroral processes at the giant planets: Energy deposition, emission mechanisms, morphology and spectra. *Space Science Reviews*, 187(1), Apr 2015. ISSN 1572-9672. doi: 10.1007/s11214-014-0042-x. URL `https://doi.org/10.1007/s11214-014-0042-x`.

B. Bézard, J. I. Moses, J. Lacy, T. Greathouse, M. Richter, and C. Griffith. Detection of Ethylene (C_2H_4) on Jupiter and Saturn in Non–Auroral Regions. In *AAS/Division for Planetary Sciences Meeting Abstracts #33*, volume 33 of *Bulletin of the American Astronomical Society*, page 1079, November 2001a.

B. Bézard, P. Drossart, T. Encrenaz, and H. Feuchtgruber. Benzene on the Giant Planets. *Icarus*, 154:492–500, December 2001b. doi: 10.1006/icar.2001.6719.

Jean-Pierre Bouanich, Ghislain Blanquet, Jacques Walrand, and Muriel Lepère. H2-broadening in the ν_7 band of ethylene by diode-laser spectroscopy. *Journal of Molecular Spectroscopy*, 218(1):22 – 27, 2003. ISSN 0022-2852. doi: https://doi.org/10.1016/S0022-2852(02)00034-6. URL `http://www.sciencedirect.com/science/article/pii/S0022285202000346`.

Jean-Pierre Bouanich, Ghislain Blanquet, Jacques Walrand, and Muriel Lepère. Hydrogen-broadening coefficients in the ν_7 band of ethylene at low temperature. *Journal of Molecular Spectroscopy*, 227(2):172 – 179, 2004. ISSN 0022-2852. doi: https://doi.org/10.1016/j.jms.2004.06.001. URL `http://www.sciencedirect.com/science/article/pii/S0022285204001924`.

J. Caldwell, F. C. Gillett, and A. T. Tokunaga. Possible infrared aurorae on Jupiter. *Icarus*, 44:667–675, December 1980. doi: 10.1016/0019-1035(80)90135-9.

J. Caldwell, A. T. Tokunaga, and G. S. Orton. Further observations of 8-micron polar brightenings of Jupiter. *Icarus*, 53:133–140, January 1983. doi: 10.1016/0019-1035(83)90026-X.

B. J. Conrath, P. J. Gierasch, and E. A. Ustinov. Thermal Structure and Para Hydrogen Fraction on the Outer Planets from Voyager IRIS Measurements. *Icarus*, 135:501–517, October 1998. doi: 10.1006/icar.1998.6000.

V. De La Haye, J. H. Waite, T. E. Cravens, I. P. Robertson, and S. Lebonnois. Coupled ion and neutral rotating model of Titan's upper atmosphere. *Icarus*, 197:110–136, September 2008. doi: 10.1016/j.icarus.2008.03.022.

P. Drossart, B. Bezard, S. K. Atreya, J. Bishop, J. H. Waite, Jr., and D. Boice. Thermal profiles in the auroral regions of Jupiter. *Journal of Geophysical Research*, 98:18803, October 1993. doi: 10.1029/93JE01801.

F. M. Flasar, V. G. Kunde, R. K. Achterberg, B. J. Conrath, A. A. Simon-Miller, C. A. Nixon, P. J. Gierasch, P. N. Romani, B. Bézard, P. Irwin, G. L. Bjoraker, J. C. Brasunas, D. E. Jennings, J. C. Pearl, M. D. Smith, G. S. Orton, L. J. Spilker, R. Carlson, S. B. Calcutt, P. L. Read, F. W. Taylor, P. Parrish, A. Barucci, R. Courtin, A. Coustenis, D. Gautier, E. Lellouch, A. Marten, R. Prangé, Y. Biraud, T. Fouchet, C. Ferrari, T. C. Owen, M. M. Abbas, R. E. Samuelson, F. Raulin, P. Ade, C. J. Césarsky, K. U. Grossman, and A. Coradini. An intense stratospheric jet on Jupiter. *Nature*, 427:132–135, January 2004.

L. N. Fletcher, B. E. Hesman, R. K. Achterberg, P. G. J. Irwin, G. Bjoraker, N. Gorius, J. Hurley, J. Sinclair, G. S. Orton, J. Legarreta, E. García-Melendo, A. Sánchez-Lavega, P. L. Read, A. A. Simon-Miller, and F. M. Flasar. The origin and evolution of saturn's 2011-2012 stratospheric vortex. *Icarus*, 221:560–586, November 2012. doi: 10.1016/j.icarus.2012.08.024.

L. N. Fletcher, T. K. Greathouse, G. S. Orton, J. A. Sinclair, R. S. Giles, P. G. J. Irwin, and T. Encrenaz. Mid-infrared mapping of Jupiter's temperatures, aerosol opacity and chemical distributions with IRTF/TEXES. *Icarus*, 278:128–161, November 2016. doi: 10.1016/j.icarus.2016.06.008.

L. N. Fletcher, G. S. Orton, J. A. Sinclair, S. Guerlet, P. Read, A. Antunano, R. Achterberg, F. M. Flasar, P. G. J. Irwin, G. Bjoraker, J. Hurley, B. Hesman, M. Segura, A. Mamoutkine, and S. Calcutt. A hexagon in saturn's northern stratosphere surrounding the emerging summertime polar vortex. *Nature Communications*, 9:3564, 2018. doi: https://doi.org/10.1038/s41467-018-06017-3.

A.I. Florescu-Mitchell and J.B.A. Mitchell. Dissociative recombination. *Physics Reports*, 430(5-6):277 – 374, 2006. ISSN 0370-1573. doi: http://dx.doi.org/10.1016/j.physrep.2006.04.002. URL `http://www.sciencedirect.com/science/article/pii/S0370157306001463`.

T. Fouchet, E. Lellouch, B. Bézard, H. Feuchtgruber, P. Drossart, and T. Encrenaz. Jupiter's hydrocarbons observed with ISO-SWS: vertical profiles of C_2H_6 and C_2H_2, detection of CH_3C_2H. *Astronomy & Astrophyrics*, 355:L13–L17, March 2000.

A. J. Friedson, A.-S. Wong, and Y. L. Yung. Models for Polar Haze Formation in Jupiter's Stratosphere. *Icarus*, 158:389–400, August 2002. doi: 10.1006/icar.2002.6885.

G. R. Gladstone, J. A. Kammer, M. H. Versteeg, T. K. Greathouse, V. Hue, J.-C. Gérard, D. Grodent, B. Bonfond, C. Jackman, G. Branduardi-Raymont, R. P. Kraft, W. R. Dunn, S. J. Bolton, J. E. P. Connerney, S. M. Levin, B. H. Mauk, P. Valek, A. Adriani, W. S. Kurth, and G. S. Orton. Juno-UVS and Chandra Observations of Jupiter's Polar Auroral Emissions. *European Planetary Science Congress*, 11:EPSC2017-388, September 2017.

A. Glasse, G. H. Rieke, E. Bauwens, M. García-Marín, M. E. Ressler, S. Rost, T. V. Tikkanen, B. Vandenbussche, and G. S. Wright. The Mid-Infrared Instrument for the James Webb Space Telescope, IX: Predicted Sensitivity. *Publications of the Astronomical Society of the Pacific*, 127:686, July 2015. doi: 10.1086/682259.

S. Guerlet, T. Fouchet, B. Bézard, A. A. Simon-Miller, and F. Michael Flasar. Vertical and meridional distribution of ethane, acetylene and propane in Saturn's stratosphere from CIRS/Cassini limb observations. *Icarus*, 203:214–232, September 2009. doi: 10.1016/j.icarus.2009.04.002.

S. Guerlet, T. Fouchet, B. Bézard, J. I. Moses, L. N. Fletcher, A. A. Simon-Miller, and F. Michael Flasar. Meridional distribution of CH_3C_2H and C_4H_2 in saturn's stratosphere from CIRS/cassini limb and nadir observations. *Icarus*, 209:682–695, October 2010. doi: 10.1016/j.icarus.2010.03.033.

S. Guerlet, T. Fouchet, S. Vinatier, A. A. Simon, E. Dartois, and A. Spiga. Stratospheric benzene and hydrocarbon aerosols detected in Saturn's auroral regions. *Astronomy & Astrophysics*, 580:A89, August 2015. doi: 10.1051/0004-6361/201424745.

R. Hanel, D. Crosby, L. Herath, D. Vanous, D. Collins, H. Creswick, C. Harris, and M. Rhodes. Infrared spectrometer for voyager. *Applied Optics*, 19:1391–1400, May 1980. doi: 10.1364/AO.19.001391.

B. E. Hesman, D. E. Jennings, P. V. Sada, G. L. Bjoraker, R. K. Achterberg, A. A. Simon-Miller, C. M. Anderson, R. J. Boyle, C. A. Nixon, L. N. Fletcher, and G. H. McCabe. Saturn's latitudinal C_2H_2 and C_2H_6 abundance profiles from Cassini/CIRS and ground-based observations. *Icarus*, 202:249–259, July 2009. doi: 10.1016/j.icarus.2009.02.013.

S. J. Houston, N. Ozak, J. Young, T. E. Cravens, and D. R. Schultz. Jovian auroral ion precipitation: Field-aligned currents and ultraviolet emissions. *Journal of Geophysical Research: Space Physics*, 123(3):2257–2273, 2018. doi: 10.1002/2017JA024872. URL `https://agupubs.onlinelibrary.wiley.com/doi/abs/10.1002/2017JA024872`.

C. J. A. Howett, P. G. J. Irwin, N. A. Teanby, A. Simon-Miller, S. B. Calcutt, L. N. Fletcher, and R. de Kok. Meridional variations in stratospheric acetylene and ethane in the southern hemisphere of the saturnian atmosphere as determined from Cassini/CIRS measurements. *Icarus*, 190:556–572, October 2007. doi: 10.1016/j.icarus.2007.03.009.

V. Hue, F. Hersant, T. Cavalié, M. Dobrijevic, and J. A. Sinclair. Photochemistry, mixing and transport in Jupiter's stratosphere constrained by Cassini. *Icarus*, 307:106–123, June 2018. doi: 10.1016/j.icarus.2018.02.018.

P. G. J. Irwin, N. A. Teanby, R. de Kok, L. N. Fletcher, C. J. A. Howett, C. C. C. Tsang, C. F. Wilson, S. B. Calcutt, C. A. Nixon, and P. D. Parrish. The NEMESIS planetary atmosphere radiative transfer and retrieval tool. *Journal of Quantitative Spectroscopy and Radiative Transfer*, 109:1136–1150, April 2008.

N. Jacquinet-Husson, N.A. Scott, A. Chédin, K. Garceran, R. Armante, A.A. Chursin, A. Barbe, M. Birk, L.R. Brown, C. Camy-Peyret, C. Claveau, C. Clerbaux, P.F. Coheur, V. Dana, L. Daumont, M.R. Debacker-Barilly, J.M. Flaud, A. Goldman, A. Hamdouni, M. Hess, D. Jacquemart, P. Köpke, J.Y. Mandin, S. Massie, S. Mikhailenko, V. Nemtchinov, A. Nikitin, D. Newnham, A. Perrin, V.I. Perevalov, L. Régalia-Jarlot, A. Rublev, F. Schreier, I. Schult, K.M. Smith, S.A. Tashkun, J.L. Teffo, R.A. Toth, Vl.G. Tyuterev, J. Vander Auwera, P. Varanasi, and G. Wagner. The 2003 edition of the geisa/iasi spectroscopic database. *Journal of Quantitative Spectroscopy and Radiative Transfer*, 95(4):429 – 467, 2005. ISSN 0022-4073. doi: https://doi.org/10.1016/j.jqsrt.2004.12.004.

N. Jacquinet-Husson, L. Crepeau, R. Armante, C. Boutammine, A. Chédin, N. A. Scott, C. Crevoisier, V. Capelle, C. Boone, N. Poulet-Crovisier, A. Barbe, A. Campargue, D. C. Benner, Y. Benilan, B. Bézard, V. Boudon, L. R. Brown, L. H. Coudert, A. Coustenis, V. Dana, V. M. Devi, S. Fally, A. Fayt, J.-M. Flaud, A. Goldman, M. Herman, G. J. Harris, D. Jacquemart, A. Jolly, I. Kleiner, A. Kleinböhl, F. Kwabia-Tchana, N. Lavrentieva, N. Lacome, L.-H. Xu, O. M. Lyulin, J.-Y. Mandin, A. Maki, S. Mikhailenko, C. E. Miller, T. Mishina, N. Moazzen-Ahmadi, H. S. P. Müller, A. Nikitin, J. Orphal, V. Perevalov, A. Perrin, D. T. Petkie, A. Predoi-Cross, C. P. Rinsland, J. J. Remedios, M. Rotger, M. A. H. Smith, K. Sung, S. Tashkun, J. Tennyson, R. A. Toth, A.-C. Vandaele, and J. Vander Auwera. The 2009 edition of the GEISA spectroscopic database. *Journal of Quantitative Spectroscopy and Radiative Transfer*, 112:2395–2445, November 2011. doi: 10.1016/j.jqsrt.2011.06.004.

S. J. Kim, J. Caldwell, A. R. Rivolo, R. Wagener, and G. S. Orton. Infrared polar brightening on Jupiter. III - Spectrometry from the Voyager 1 IRIS experiment. *Icarus*, 64:233–248, November 1985. doi: 10.1016/0019-1035(85)90088-0.

T. T. Koskinen, J. I. Moses, R. A. West, S. Guerlet, and A. Jouchoux. The detection of benzene in saturn's upper atmosphere. *Geophysical Research Letters*, 43(15):7895–7901, 2016. ISSN 1944-8007. doi: 10.1002/2016GL070000. 2016GL070000.

T. Kostiuk, P. Romani, F. Espenak, and T. A. Livengood. Temperature and abundances in the Jovian auroral stratosphere. 2: Ethylene as a probe of the microbar region. *Journal of Geophysical Research*, 98:18823, October 1993. doi: 10.1029/93JE01332.

V. A. Krasnopolsky. A photochemical model of Titan's atmosphere and ionosphere. *Icarus*, 201:226–256, May 2009. doi: 10.1016/j.icarus.2008.12.038.

V. G. Kunde, P. A. Ade, R. D. Barney, D. Bergman, J.-F. Bonnal, R. Borelli, D. Boyd, J. C. Brasunas, G. Brown, S. B. Calcutt, F. Carroll, R. Courtin, J. Cretolle, J. A. Crooke, M. A. Davis, S. Edberg, R. Fettig, M. Flasar, D. A. Glenar, S. Graham, J. G. Hagopian, C. F. Hakun, P. A. Hayes, L. Herath, L. Horn, D. E. Jennings, G. Karpati, C. Kellebenz, B. Lakew, J. Lindsay, J. Lohr, J. J. Lyons, R. J. Martineau, A. J. Martino, M. Matsumura, J. McCloskey, T. Melak, G. Michel, A. Morell, C. Mosier, L. Pack, M. Plants, D. Robinson, L. Rodriguez, P. Romani, W. J. Schaefer, S. Schmidt, C. Trujillo, T. Vellacott, K. Wagner, and D. Yun. Cassini infrared Fourier spectroscopic investigation. In L. Horn, editor, *Society of Photo-Optical Instrumentation Engineers (SPIE) Conference Series*, volume 2803 of *Society of Photo-Optical Instrumentation Engineers (SPIE) Conference Series*, pages 162–177, October 1996.

A. A. Lacis and V. Oinas. A description of the correlated-k distribution method for modelling nongray gaseous absorption, thermal emission, and multiple scattering in vertically inhomogeneous atmospheres. *Journal of Geophysical Research*, 96:9027–9064, may 1991. doi: 10.1029/90JD01945.

J. H. Lacy, M. J. Richter, T. K. Greathouse, D. T. Jaffe, and Q. Zhu. Texes: A sensitive high-resolution grating spectrograph for the mid-infrared. *Publications of the Astronomical Society of the Pacific*, 114:153–168, February 2002. doi: 10.1086/338730.

T. A. Livengood, T. Kostiuk, and F. Espenak. Temperature and abundances in the Jovian auroral stratosphere. 1: Ethane as a probe of the millibar region. *Journal of Geophysical Research*, 98:18813, October 1993. doi: 10.1029/93JE01043.

H. Melin, L. N. Fletcher, P. T. Donnelly, T. K. Greathouse, J. H. Lacy, G. S. Orton, R. S. Giles, J. A. Sinclair, and P. G. J. Irwin. Assessing the long-term variability of acetylene and ethane in the stratosphere of Jupiter. *Icarus*, 305:301–313, May 2018. doi: 10.1016/j.icarus.2017.12.041.

P. F. Morrissey, P. D. Feldman, M. A. McGrath, B. C. Wolven, and H. W. Moos. The Ultraviolet Reflectivity of Jupiter at 3.5 Angstrom Resolution from Astro-1 and Astro-2. *The Astrophysical Journal Letters*, 454:L65, November 1995. doi: 10.1086/309763.

J. I. Moses and T. K. Greathouse. Latitudinal and seasonal models of stratospheric photochemistry on Saturn: Comparison with infrared data from IRTF/TEXES. *Journal of Geophysical Research (Planets)*, 110:E09007, September 2005. doi: 10.1029/2005JE002450.

J. I. Moses, B. Bézard, E. Lellouch, G. R. Gladstone, H. Feuchtgruber, and M. Allen. Photochemistry of Saturn's Atmosphere. I. Hydrocarbon Chemistry and Comparisons with ISO Observations. *Icarus*, 143:244–298,

February 2000. doi: 10.1006/icar.1999.6270.

J. I. Moses, T. Fouchet, B. Bézard, G. R. Gladstone, E. Lellouch, and H. Feuchtgruber. Photochemistry and diffusion in Jupiter's stratosphere: Constraints from ISO observations and comparisons with other giant planets. *Journal of Geophysical Research (Planets)*, 110:E08001, August 2005. doi: 10.1029/2005JE002411.

H. B. Niemann, S. K. Atreya, G. R. Carignan, T. M. Donahue, J. A. Haberman, D. N. Harpold, R. E. Hartle, D. M. Hunten, W. T. Kasprzak, P. R. Mahaffy, T. C. Owen, and S. H. Way. The composition of the Jovian atmosphere as determined by the Galileo probe mass spectrometer. *Journal of Geophysical Research*, 103:22831–22846, September 1998. doi: 10.1029/98JE01050.

C. A. Nixon, R. K. Achterberg, B. J. Conrath, P. G. J. Irwin, N. A. Teanby, T. Fouchet, P. D. Parrish, P. N. Romani, M. Abbas, A. LeClair, D. Strobel, A. A. Simon-Miller, D. J. Jennings, F. M. Flasar, and V. G. Kunde. Meridional variations of C_2H_2 and C_2H_6 in Jupiter's atmosphere from Cassini CIRS infrared spectra. *Icarus*, 188:47–71, May 2007. doi: 10.1016/j.icarus.2006.11.016.

C. A. Nixon, R. K. Achterberg, P. N. Romani, M. Allen, X. Zhang, N. A. Teanby, P. G. J. Irwin, and F. M. Flasar. Abundances of Jupiter's trace hydrocarbons from Voyager and Cassini. *Planetary & Space Science*, 58: 1667–1680, November 2010. doi: 10.1016/j.pss.2010.05.008.

J. Norwood, H. Hammel, S. Milam, J. Stansberry, J. Lunine, N. Chanover, D. Hines, G. Sonneborn, M. Tiscareno, M. Brown, and P. Ferruit. Solar System Observations with the James Webb Space Telescope. *Publications of the Astronomical Society of Pacific*, 128(2):025004, February 2016. doi: 10.1088/1538-3873/128/960/025004.

N. Ozak, D. R. Schultz, T. E. Cravens, V. Kharchenko, and Y.-W. Hui. Auroral x-ray emission at jupiter: Depth effects. *Journal of Geophysical Research: Space Physics*, 115(A11):A11306, 2010. doi: 10.1029/2010JA015635. URL `https://agupubs.onlinelibrary.wiley.com/doi/abs/10.1029/2010JA015635`.

W. H. Press, S. A. Teukolsky, W. T. Vetterling, and B. P. Flannery. *Numerical recipes in FORTRAN. The art of scientific computing*. 1992.

W. R. Pryor and C. W. Hord. A study of photopolarimeter system UV absorption data on Jupiter, Saturn, Uranus, and Neptune - Implications for auroral haze formation. *Icarus*, 91:161–172, May 1991. doi: 10.1016/0019-1035(91)90135-G.

G. H. Rieke, G. S. Wright, T. Böker, J. Bouwman, L. Colina, A. Glasse, K. D. Gordon, T. P. Greene, M. Güdel, T. Henning, K. Justtanont, P.-O. Lagage, M. E. Meixner, H.-U. Nørgaard-Nielsen, T. P. Ray, M. E. Ressler, E. F. van Dishoeck, and C. Waelkens. The Mid-Infrared Instrument for the James Webb Space Telescope, I: Introduction. *Publications of the Astronomical Society of the Pacific*, 127:584, July 2015. doi: 10.1086/682252.

P. N. Romani. Recent Rate Constant and Product Measurements of the Reactions C_2H_3 + $H_2$and C_2H_3 + H - Importance for Photochemical Modeling of Hydrocarbons on Jupiter. *Icarus*, 122:233–241, August 1996. doi: 10.1006/icar.1996.0122.

J. A. Sinclair, P. G. J. Irwin, L. N. Fletcher, J. I. Moses, T. K. Greathouse, A. J. Friedson, B. Hesman, J. Hurley, and C. Merlet. Seasonal variations of temperature, acetylene and ethane in Saturn's atmosphere from 2005 to 2010, as observed by Cassini-CIRS. *Icarus*, 225:257–271, July 2013. doi: 10.1016/j.icarus.2013.03.011.

J. A. Sinclair, P. G. J. Irwin, L. N. Fletcher, T. Greathouse, S. Guerlet, J. Hurley, and C. Merlet. From Voyager-IRIS to Cassini-CIRS: Interannual variability in Saturn's stratosphere? *Icarus*, 233:281–292, May 2014.

J. A. Sinclair, G. Orton, Y. Kasaba, T. M. Sato, C. Tao, J. H. Waite, T. Cravens, S. Houston, L. Fletcher, P. Irwin, and T. K. Greathouse. Solar wind control of stratospheric temperatures in Jupiter's auroral regions? In *AAS/Division for Planetary Sciences Meeting Abstracts #49*, volume 49 of *AAS/Division for Planetary Sciences Meeting Abstracts*, page 211.02, October 2017.

J. A. Sinclair, G. S. Orton, T. K. Greathouse, Moses Fletcher, L. N., J. I., V. Hue, and P. G. J Irwin. Jupiter's auroral-related stratospheric heating and chemistry I: analysis of Voyager-IRIS and Cassini-CIRS spectra. *Icarus*, 292:182–207, January 2017a. doi: http://dx.doi.org/10.1016/j.icarus.2016.12.033.

J. A. Sinclair, G. S. Orton, T. K. Greathouse, Moses Fletcher, L. N., J. I., V. Hue, and P. G. J Irwin. Independent evolution of stratospheric temperatures in Jupiter's northern and southern auroral regions from 2014 to 2016. *Geophysical Research Letters*, 44:5345–5354, June 2017b. doi: doi:10.1002/2017GL073529.

J. A. Sinclair, G. S. Orton, T. K. Greathouse, Moses Fletcher, L. N., J. I., V. Hue, and P. G. J Irwin. Jupiter's auroral-related stratospheric heating and chemistry II: analysis of IRTF-TEXES spectra measured in December 2014. *Icarus*, 300:305–326, January 2018.

V. Vuitton, R. V. Yelle, and M. J. McEwan. Ion chemistry and N-containing molecules in Titan's upper atmosphere. *Icarus*, 191:722–742, November 2007. doi: 10.1016/j.icarus.2007.06.023.

V. Vuitton, R. V. Yelle, and J. Cui. Formation and distribution of benzene on Titan. *Journal of Geophysical Research (Planets)*, 113:E05007, May 2008. doi: 10.1029/2007JE002997.

L. Waschull, Y. Heiner, and H.-D. Kronfeldt. Diode laser spectroscopy in the 9.8-μm ν_14 band of benzene. ii. self-, air-, and noble-gas broadening coefficients. *Journal of Molecular Spectroscopy*, 190:140–149, 1998.

R. A. West, D. Griswold, and C. Porco. Jupiter's Polar UV Great Dark Spot. In *AAS/Division for Planetary Sciences Meeting Abstracts 35*, volume 35 of *Bulletin of the American Astronomical Society*, page 1009, May 2003.

E. H. Wilson and S. K. Atreya. Current state of modeling the photochemistry of Titan's mutually dependent atmosphere and ionosphere. *Journal of Geophysical Research (Planets)*, 109:E06002, June 2004. doi: 10.1029/2003JE002181.

A.-S. Wong, A. Y. T. Lee, Y. L. Yung, and J. M. Ajello. Jupiter: Aerosol Chemistry in the Polar Atmosphere. *Astrophysical Journal Letters*, 534: L215–L217, May 2000. doi: 10.1086/312675.

A.-S. Wong, Y. L. Yung, and A. J. Friedson. Benzene and Haze Formation in the Polar Atmosphere of Jupiter. *Geophysical Research Letters*, 30:1447, April 2003. doi: 10.1029/2002GL016661.

Appendix A. IRIS $\Delta\tilde{\nu}$=4.3 cm^{-1}, CIRS $\Delta\tilde{\nu}$=0.5 cm^{-1}

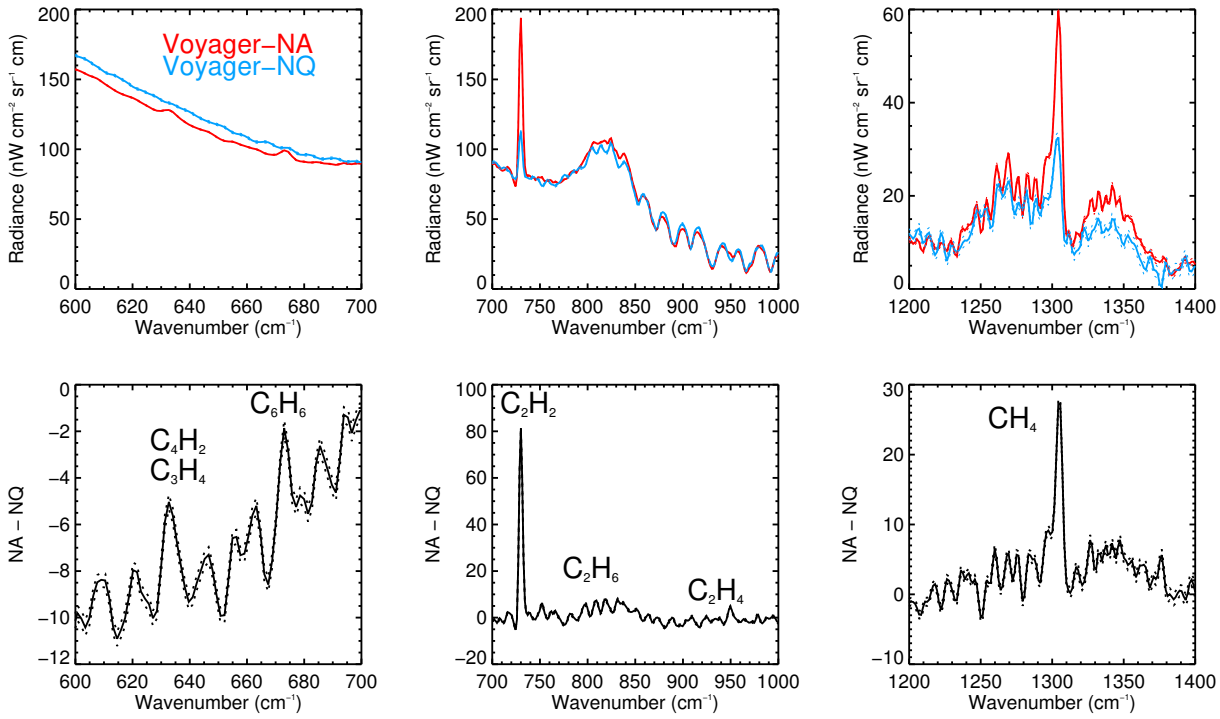

Figure A.9: The top row shows the Voyager-NA (red) and Voyager-NQ (blue) coadded spectra (solid) which respectively represent an auroral and quiescent region at Jupiter's high-northern latitudes. 1-σ noise levels are shown as dotted lines of the same color. The bottom row shows the residual between the Voyager-NA and Voyager-NQ spectra (solid) and uncertainty (dotted, computed by adding the noise on the spectra in quadrature). Spectra and residual spectra are shown over three wavenumber ranges, which capture the spectral emission of the target minor species, as well as CH_4, C_2H_2 and C_2H_6. This plot was initially presented in Sinclair et al. (2017a) but is also included in this paper for reference.

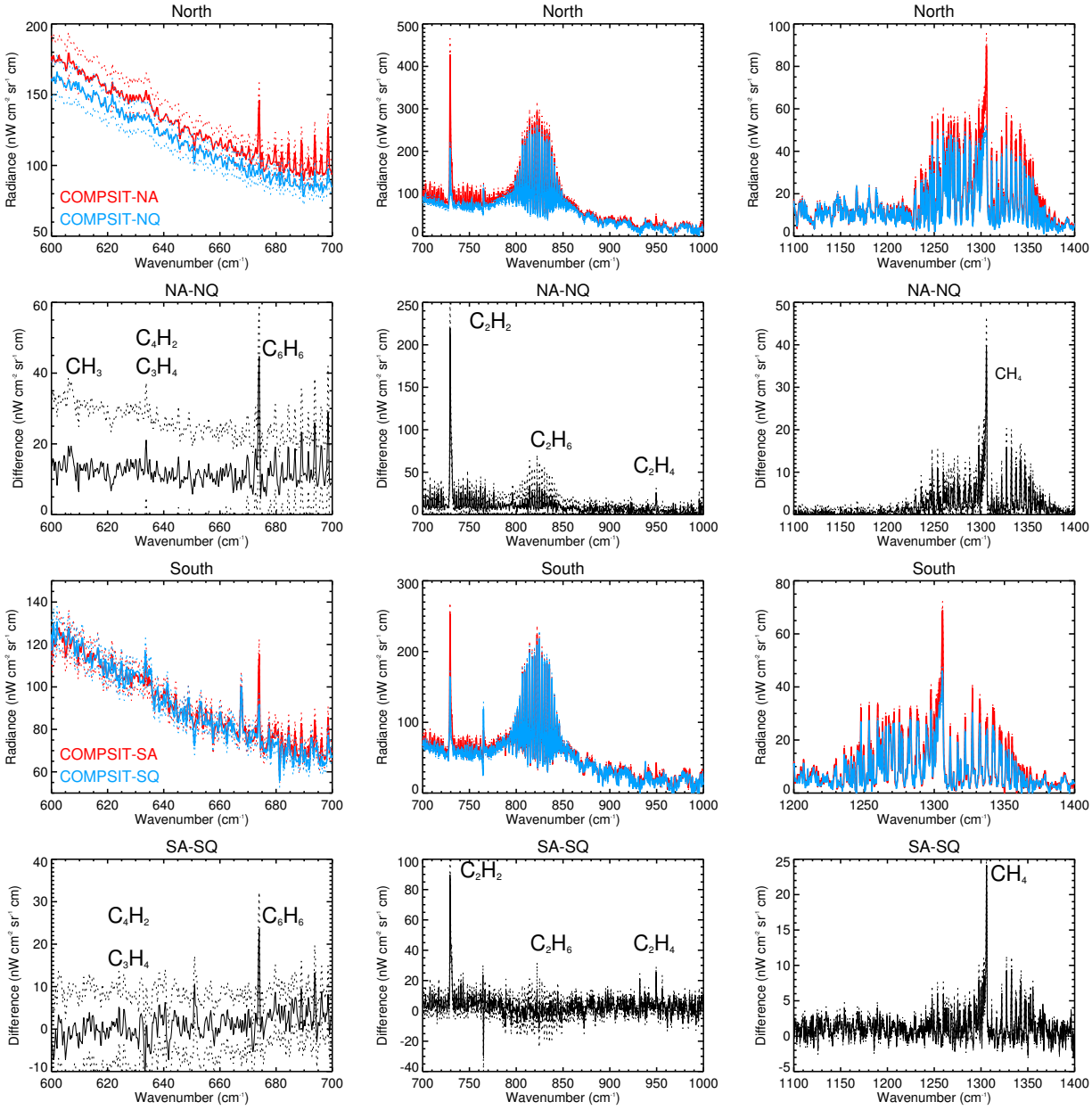

Figure A.10: The top row shows the COMPSIT-NA (red) and COMPSIT-NQ (blue) coadded spectra (solid) which respectively represent an auroral and quiescent region at Jupiter's high-northern latitudes. 1-σ noise levels are shown as dotted lines of the same color. The 2nd row shows the residual between the COMPSIT-NA and COMPSIT-NQ spectra (solid) and uncertainty (dotted, computed by adding the noise on the spectra in quadrature). The 3rd and 4th similarly show the COMPSIT-SA and COMPSIT-SQ spectra and their residual. Spectra and residual spectra are shown over three wavenumber ranges, which capture the spectral emission of the target minor species, as well as CH_4, C_2H_2 and C_2H_6. This plot was initially presented in Sinclair et al. (2017a) but is also included in this paper for reference.

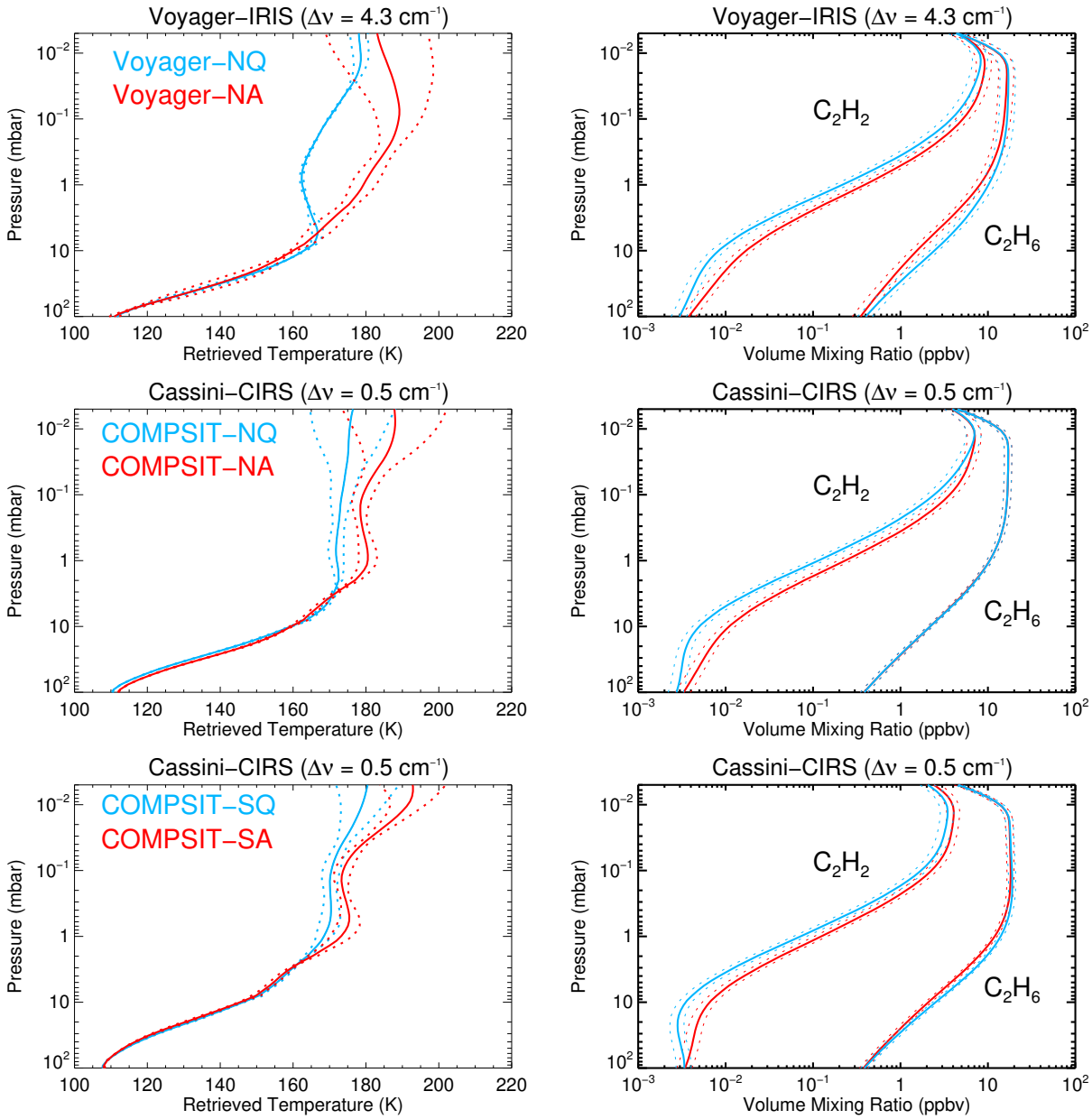

Figure A.11: Retrieved vertical profiles of temperature (left column) and volume mixing ratios of C_2H_2 and C_2H_6 (right column) for Voyager-NA/NQ (top row), COMPSIT-NQ/NA (middle row) and COMPSIT-SQ/SA (bottom row). Solid and dotted lines mark the profile and 1-σ uncertainty, respectively.

Appendix B. CIRS $\Delta\tilde{\nu}$=2.5 cm^{-1}

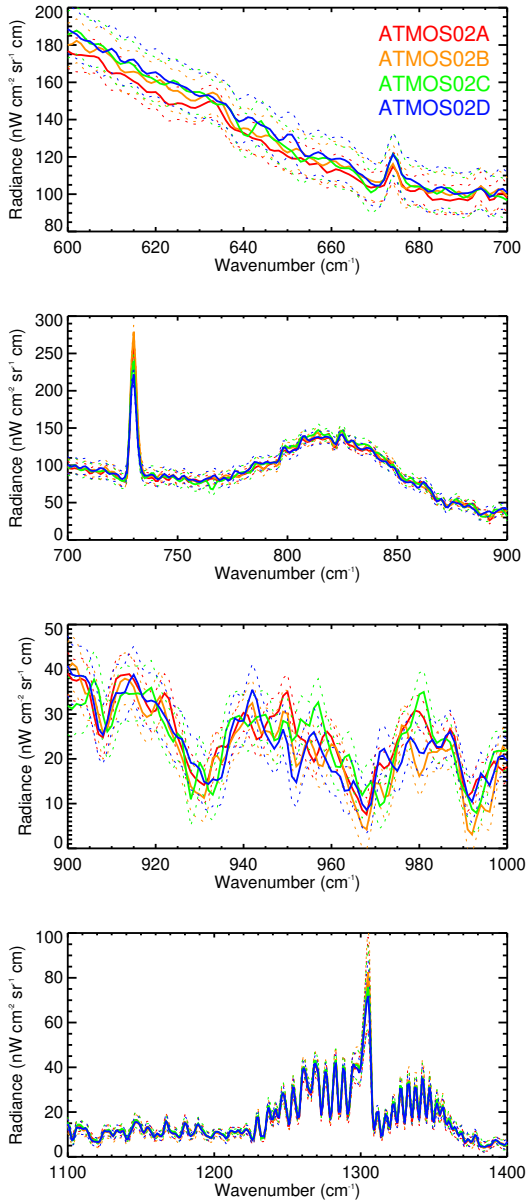

Figure B.12: Cassini-CIRS $\Delta\tilde{\nu}$ = 2.5 cm^{-1} spectra of Jupiter's northern auroral region (coadded from 60-80°N, 150-210°W) from the ATMOS02A (red), ATMOS02B (orange), ATMOS02C (green) and ATMOS02D (blue) datasets. Spectra are shown as solid lines. The 1-σ noise level is shown as the dotted line.

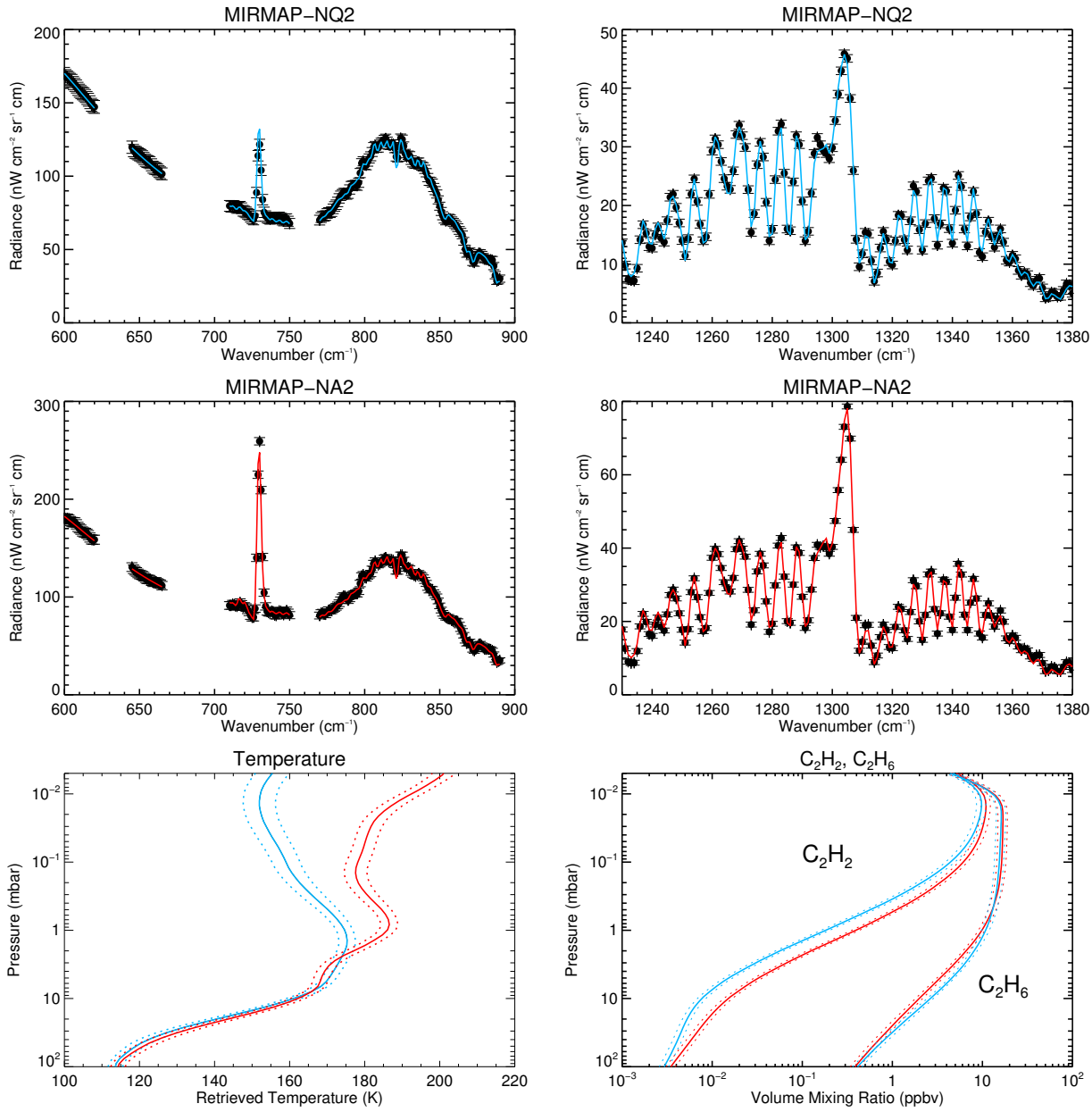

Figure B.13: Model-spectral comparisons of MIRMAP-NQ2 (top row) and MIRMAP-NA2 (middle row) from 600 - 900 cm^{-1} (left column) and 1230 - 1380 cm^{-1} (right column). Observed spectra are shown as black points with error bars, modelled spectra are shown as solid lines in blue for MIRMAP-NQ2 and red for MIRMAP-NA2. The corresponding retrieved vertical profiles are shown in the bottom row for temperature (left) and the volume mixing ratios of C_2H_2 and C_2H_6 (right). Solid lines are retrieved profiles and dotted lines mark the 1-σ retrieval confidence.